Structure-based Design and Discovery of Pyridyl-bearing Fused Bicyclic HIV-1 Inhibitors: Synthesis, Biological Characterization, and Molecular Modeling Studies

Boshi Huang,[†,§] Tiziana Ginex,[‡] F. Javier Luque,[‡] Xiangyi Jiang,[†] Ping Gao,[†] Jian Zhang,[†] Dongwei Kang,[†,⊥] Dirk Daelemans,[#] Erik De Clercq,[#] Christophe Pannecouque,[#] Peng Zhan,[†,⊥,*] and Xinyong Liu[†,⊥,*]

[†] *Department of Medicinal Chemistry, Key Laboratory of Chemical Biology (Ministry of Education), School of Pharmaceutical Sciences, Cheeloo College of Medicine, Shandong University, 44 West Culture Road, 250012 Jinan, Shandong, PR China*

[‡] *Department of Nutrition, Food Science and Gastronomy, Faculty of Pharmacy, Campus Torribera, Institute of Biomedicine (IBUB) and Institute of Theoretical and Computational Chemistry (IQTCUB), University of Barcelona, 08921 Santa Coloma de Gramenet, Spain*

[#] *Rega Institute for Medical Research, Laboratory of Virology and Chemotherapy, K.U.Leuven, Herestraat 49 Postbus 1043 (09.A097), B-3000 Leuven, Belgium*

[⊥] *China-Belgium Collaborative Research Center for Innovative Antiviral Drugs of Shandong Province, 44 West Culture Road, 250012, Jinan, Shandong, PR China*

ABSTRACT

Two series of new pyridyl-bearing fused bicyclic analogues designed to target the dual tolerant regions of the non-nucleoside reverse transcriptase inhibitor (NNRTI) binding pocket were synthesized and evaluated for their anti-HIV activities. Several compounds, such as **6**, **14**, **15**, **21**, **30**, and **33,** were found to be potent inhibitors against wild-type (WT) HIV-1 strain or multiple NNRTI-resistant strains at low nanomolar levels. Detailed structure−activity relationships were obtained by utilizing the variation of moieties within the corresponding pharmacophores. In vitro metabolic stability profiles and some drug-like properties of selected compounds were assessed, furnishing preliminary structure-metabolic stability relationships. Furthermore, molecular modeling studies elucidated the binding modes of compounds **6**, **15**, **21**, and **30** in the binding pocket of WT, E138K, K103N, or Y181C HIV-1 RTs. These promising compounds can be used as lead compounds and warrant further structural optimization to yield more active HIV-1 inhibitors.

INTRODUCTION

HIV-1 reverse transcriptase (RT) is a well-established target to treat HIV-1 infections.[1] Currently, RT inhibitors with two distinct mechanism of action are widely used in the highly active antiretroviral therapy (HAART).[2] Nucleoside RT inhibitors (NRTIs) are incorporated in the viral DNA generating premature strand termination,

while the non-nucleoside RT inhibitors (NNRTIs) function by causing a large conformational change as binding to an allosteric pocket (NNRTI binding pocket, NNIBP) in the vicinity of the polymerase active site.[3] Up to now, there are five NNRTI drugs approved by U.S. FDA and currently used in anti-HIV therapy: nevirapine (NVP), efavirenz (EFV), etravirine (ETR), rilpivirine (RPV), and doravirine (DOR) (Figure 1). NNRTIs are key components of HAART, which consists of the most successful antiviral combination therapies Atripla (EFV/emtricitabine/tenofovir disoproxil fumarate) and Complera (RPV/emtricitabine/tenofovir disoproxil fumarate).[4, 5] However, emergence of drug resistance to clinically utilized NNRTIs, especially to the first-generation drugs, continues to be a major cause of treatment failure.[6]

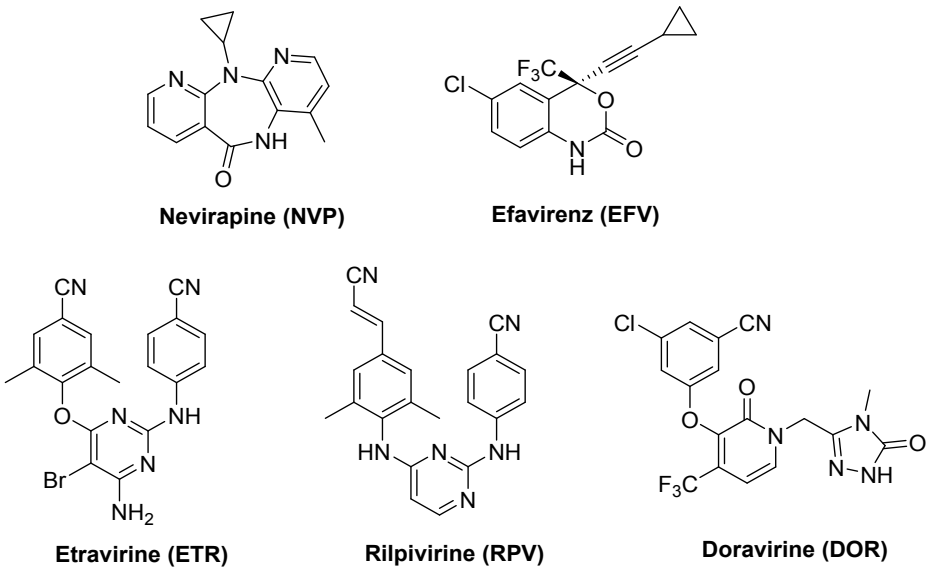

Figure 1. Chemical structures of HIV-1 NNRTIs approved by U.S. FDA and currently used in anti-HIV therapy.

To address this major issue, two second-generation NNRTI drugs, ETR and RPV with a flexible diarylpyrimidine scaffold were successfully developed.[7, 8] Both drugs maintain robust potency over a variety of mutant HIV-1 strains which are resistant to early NNRTIs, including K103N, Y181C, and the most frequently encountered K103N/Y181C double mutant strain (Figure 1).[9] Nevertheless, due to the high mutation rate and the lack of intrinsic proofreading exonuclease activity of HIV-1 RT, new resistance profiles associated with ETR and RPV, such as E138K, have been observed in clinical trials.[10, 11] Consequently, the rapid selection of resistance mutations necessitates the development of new generation NNRTIs that are effective against resistance-associated variants of HIV-1 RT.

The X-ray crystallographic analysis and previous structure-activity relationship (SAR) studies have corroborated that the diarylpyrimidine derivatives generally contained three pivotal pharmacophores (Figure 2):[9, 12-14] an aminobenzonitrile moiety (A-ring), a central ring containing a hydrogen bond acceptor or donor (B-ring) that forms a hydrogen bond with K101, and a 2,4,6-trisubstituted phenoxy moiety (C-ring). The A-ring is connected to the B-ring through the *NH* linker that has been demonstrated to establish another hydrogen bond with K101. The dual hydrogen bonds formed between the diarylpyrimidine derivatives and K101 have been proven essential to maintain their high binding affinities.[12] Additionally, the A-ring moiety locates in a solvent-exposed region termed “tolerant region I”, which is composed of amino acid residues K103, V106, F227, Y318, and P236. As is well known, a widely

accepted medicinal chemistry strategy to improve the potency and anti-resistance profile of an NNRTI against HIV-1 strains is to establish strong interactions of the small molecule with conserved regions of the NNIBP, such as main chain atom(s) and/or highly conserved side chain residues.[15] In this regard, the *NH* linker and the N atom of the B-ring of the designed ligands were kept to generate the key dual hydrogen bonds with the K101 backbone moieties, which could be beneficial for maintaining antiviral potency against WT and drug-resistant HIV-1 strains. Another N atom was introduced onto the A-ring of diarylpyrimidines to explore the chemical space of tolerant region I. More importantly, introducing nitrogen atom shows great promise to produce ameliorated drug-like properties of diarylpyrimidine derivatives,[16] since this class of HIV-1 inhibitors are most likely endowed with poor water solubility and low bioavailability.[17, 18]

Furthermore, another open region of NNIBP, namely the "NNRTI entrance channel" or "tolerant region II", defined by K101, E138 and V179, has been recently disclosed and preliminarily exploited in NNRTI research.[19, 20] Upon examination of the binding mode of ETR or RPV in their co-crystal complexes with HIV-1 RT,[12] we found that the 5 and 6 position of the central pyrimidine ring of diarylpyrimidines exactly orientated towards the solvent-exposed tolerant region II, which seemed to be capable of accommodating favorable moieties. It was therefore speculated that cyclization of the 5 and 6 position of the pyrimidine ring, i.e., an additional ring being fused with the pyrimidine ring, may possibly generate extra interactions with the

surrounding residues of the tolerant region II of NNIBP and simultaneously elevate the potency and anti-resistance profiles.

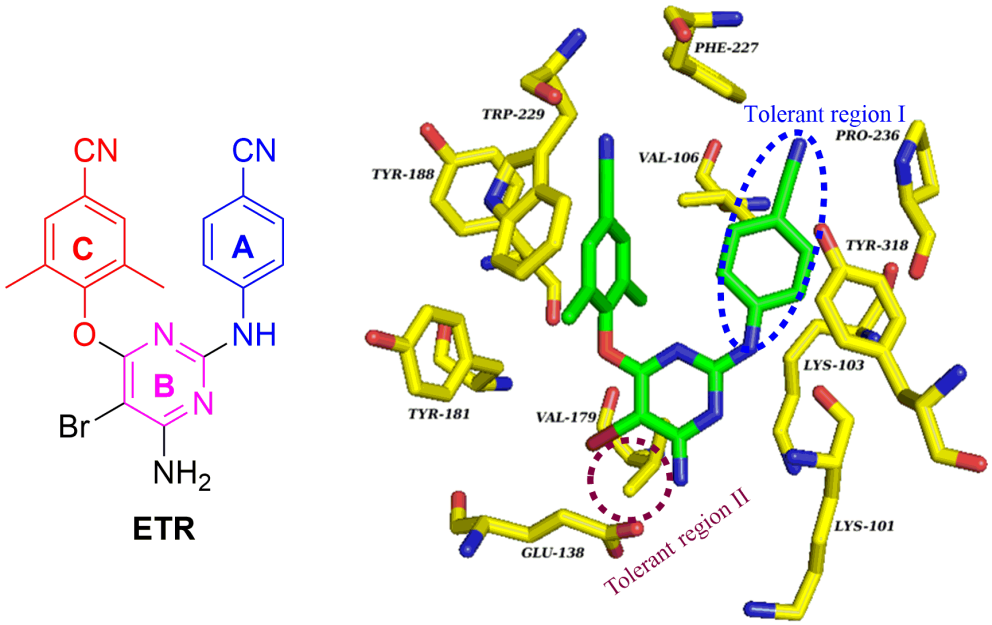

Figure 2. The illustration of pharmacophore model of ETR and the co-crystal structure of ETR/WT HIV-1 RT (PDB code: 3MEC). The co-crystal structure figure was generated using PyMOL (www.pymol.org).

Extensive research conducted in our laboratory and others in the last decade have led to the discovery of several diarylpyrimidine-typed HIV-1 NNRTIs targeting the tolerant region I and/or the tolerant region II of NNIBP with remarkably improved anti-resistance profiles, as well as desirable drug-like properties (Figure 3).[10, 18, 21-24] These results have confirmed the feasibility of rational molecular design of new "multi-sites binding" NNRTIs targeting the dual tolerant regions of NNIBP.

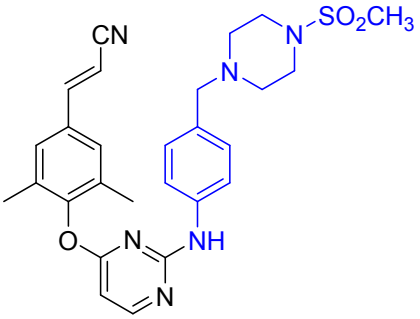

BH-11c
EC_{50} (nM) = 3.5 (WT), 3.6 (K103N),
7.5 (E138K), 25 (Y181C)
S = 30.92 mg/mL (pH 7.0)

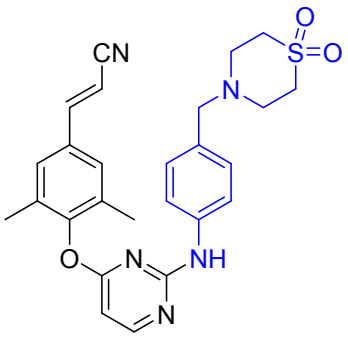

XJ-10c
EC_{50} (nM) = 2.1 (WT), 1.9 (K103N),
7.5 (E138K), 33 (Y181C)
S = 34.0 mg/mL (pH 7.0)

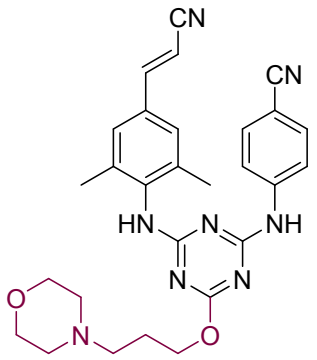

MB-4d
EC_{50} (nM) = 1.2 (WT), 12 (Y181C),
1.3 (K103N/Y181C)
S = 14.2 mg/mL (pH 6.5)

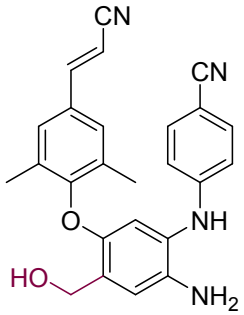

LS-14h
EC_{50} (nM) = 0.53 (WT), 3.4 (K101E),
3.9 (E138K)
S = 20.9 mg/mL (pH 2.0)

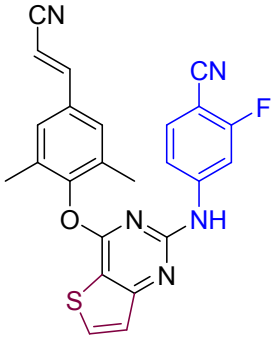

DK-24b
EC_{50} (nM) = 8.6 (WT), < 3.6 (L100I),
< 3.6 (K103N), 8.4 (Y181C),
8.1 (Y188L), 9.4 (E138K)
9.2 (F227L/V106A)
21.5 (K103N/Y181C)
hERG inhibitory activity IC_{50} > 30 μM

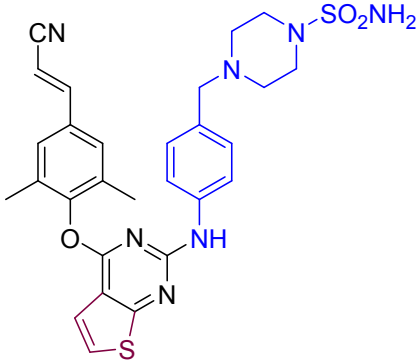

YS-16b1
EC_{50} (nM) = 8 (WT), 15 (L100I),
7 (K103N), 25 (E138K)
S = 49.3 mg/mL (pH 7.0)

Figure 3. Some representative diarylpyrimidine-typed HIV-1 NNRTIs targeting the tolerant region I and/or the tolerant region II of NNIBP.

In continuation of our own efforts on the development of next generation NNRTIs, we designed and synthesized two series of pyridyl-bearing fused bicyclic derivatives (Figure 4), in which the right benzene ring was replaced with pyridine ring (introduction of one nitrogen atom, **A**). Meanwhile, the cyclohexyl moiety with a large molecular volume (102.60 A^3, predicted by free online software Molinspiration) was first proposed to be installed as fused ring with the pyrimidine ring (**B**), which was anticipated to occupy the tolerant region II more effectively. More importantly, introduction of the saturated fragment, i.e. cyclohexyl moiety, may increase the Fsp^3 metric (fraction of sp^3 carbon atoms, the number of sp^3 hybridized carbons/total carbon count) that has been an emerging indicator of drug-likeness of lead compounds.[25, 26] It is observed that ETR (Fsp^3 = 0.10) and RPV (Fsp^3 = 0.09) have low Fsp^3 contents due to the three aromatic rings. Different substituents were further introduced into the position where the right cyano group was to examine their influence on antiretroviral potency as well (series I).

Moreover, based on the SARs derived from series I of synthesized small molecules, we subsequently employed a scaffold hopping strategy to rationally design the second series of target compounds. These compounds featured one nitrogen atom containing five-membered ring fused with the pyrimidine ring, which hydrophilic groups hydroxymethyl and *N*-acetylmorpholinyl were further introduced into the five-membered ring to generate additional possible interactions with the surrounding

residues in the tolerant region II (**B**) (series II). It should be mentioned that we employed a nitrogen-walk approach[16] in the two counterparts of series II of designed compounds, allowing for introducing additional moieties onto the nitrogen atom of the fused five-membered ring.

On the other hand, since most metabolizing enzymes in the liver (e.g. cytochrome P450, CYP) are responsible for the majority of drug metabolism in vivo and binding pockets in CYP enzymes are hydrophobic,[27] we expected that the installation of the fused five-membered ring and hydrophilic moieties would be favorable for decreasing ClogP values and therefore may increase the metabolism stability profiles of the designed compounds. In addition, the preferred 2,4,6-trisubstitued moiety was kept at the left-wing portion (**C**) of these newly designed target compounds. In this design scenario, all the key interactions between the small molecules and the important residues in the binding pocket could be maintained, while new interactions (targeting the dual tolerant regions) can be formed.

In the present study, we report the multidimensional optimization, structure-activity relationships, in vitro metabolic stability profiles, and molecular modeling results of the newly designed pyridyl-bearing fused bicyclic derivatives.

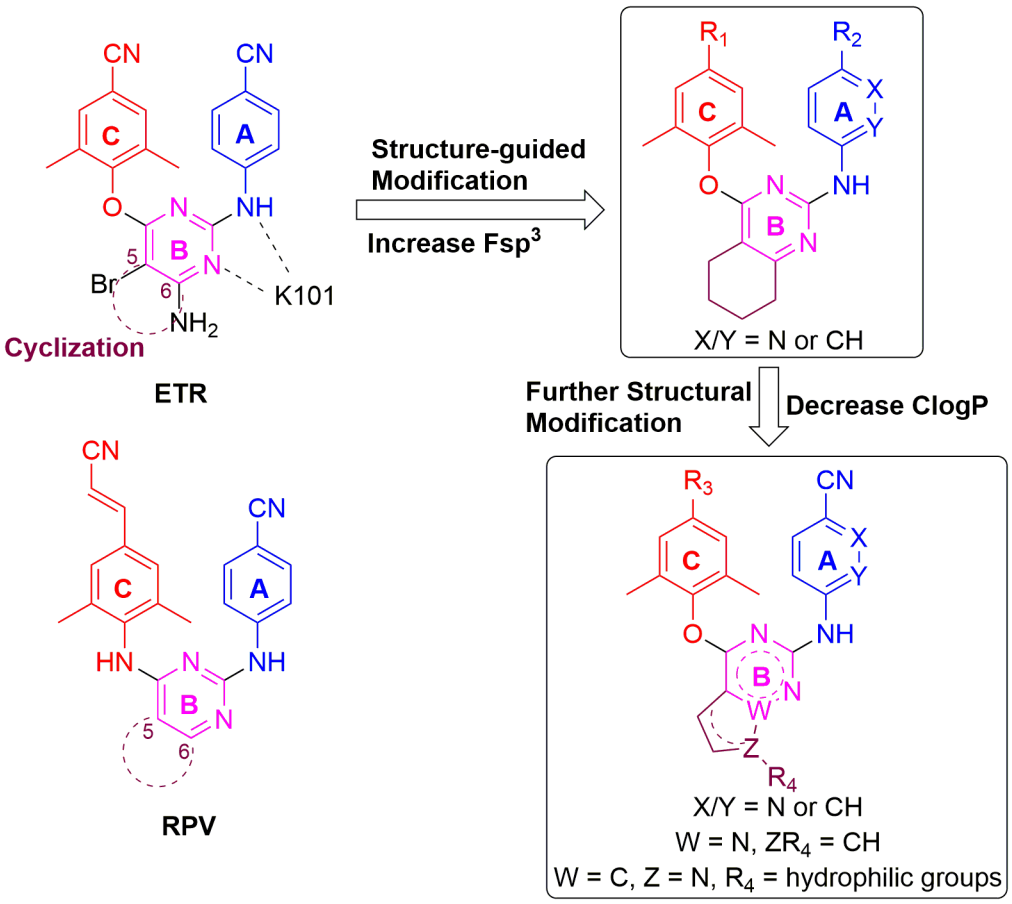

Figure 4. Structure-guided drug design and modification of pyridyl-bearing fused bicyclic derivatives.

CHEMISTRY

The synthetic routes for the newly designed target compounds are proposed and shown in Scheme 1, Scheme 2, Scheme 3 and Scheme 4. As depicted in Scheme 1, the starting material ethyl 2-oxocyclohexanecarboxylate (**1**) was easily converted to 5,6,7,8-tetrahydroquinazoline-2,4-diol (**2**).[28] Chlorination of **2** using phosphorous oxychloride generated 2,4-dichloro-5,6,7,8-tetrahydroquinazoline (**3**).[28] Coupling of the intermediate **3** with 2,4,6-trisubstituted phenols afforded the key intermediates

4a-c.[18] **4a-c** underwent a Buchwald-Hartwig reaction with commercially available substituted anilines or 5-aminopicolinonitrile or 6-aminonicotinonitrile to provide the target compounds **5-13**.[18] Furthermore, through Wittig-Horner reaction, the aldehyde-containing compounds were treated with diethyl cyanomethylphosphonate in tetrahydrofuran to readily give the cyanovinyl substituted target compounds **14-16**.[29]

As shown in Scheme 2, target compounds **20** and **21** were obtained in three steps from pyrrolo[2,1-f][1,2,4]triazine-2,4-diol (**17**) following similar procedures as employed in Scheme 1, while different catalyst and ligand were utilized in the Buchwald-Hartwig reaction. Treatment of **20** with phosphorous oxychloride at 40℃ yielded the target compound **22** bearing a 4'-cyanovinyl group.[30]

Scheme 3 illustrates the synthesis of compounds **26-31**. The starting material dichloro-7*H*-pyrrolo[2,3-d]pyrimidine (**23**) reacted with (2-(chloromethoxy)ethyl)trimethylsilane (SEM-Cl) to give 2,4-dichloro-7-((2-(trimethylsilyl)ethoxy)methyl)-7*H*-pyrrolo[2,3-d]pyrimidine (**24**).[31] **24** underwent two steps of nucleophilic aromatic substitution reactions that were similar to those described in Scheme 1, providing the target compounds **26-28**. Treatment of **26-28** with trifluoroacetic acid in methylene chloride furnished the corresponding hydroxymethyl containing target compounds **29-31**.[32]

As illustrated in Scheme 4, the target compound **33** was synthesized from the well-prepared compound **32** that has been previously reported by our group[33] and

4-(chloroacetyl)morpholine. To confirm that the regioselective substitution reaction occurred at the *NH* group of the pyrrole ring to generate **33**, not at the right *NH* linker to form compound **34**, we further performed 2D NMR determination, including DEPT135, HSQC and HMBC experiments (See Supporting Information). The DEPT135 spectrum combined with HSQC confirmed CH=CH at positions 5 and 6 of the pyrrole ring (δ_C: 128.22 and 98.10 ppm, δ_H: 7.27 and 6.56 ppm). It is clear from 1D NMR that the protons of the methylene group next to the carbonyl group has a shift value (δ) at 5.19 as a singlet. The HMBC spectrum identified the connections of the protons of this specific methylene group with three carbons at δ 128.22, 154.84 and 166.06 ppm. Taken together, δ_C 128.22 is for C_6 of the pyrrole ring, and the structure of compound **33** was confirmed.

Scheme 1. Synthesis of Target Compounds 5-16[a]

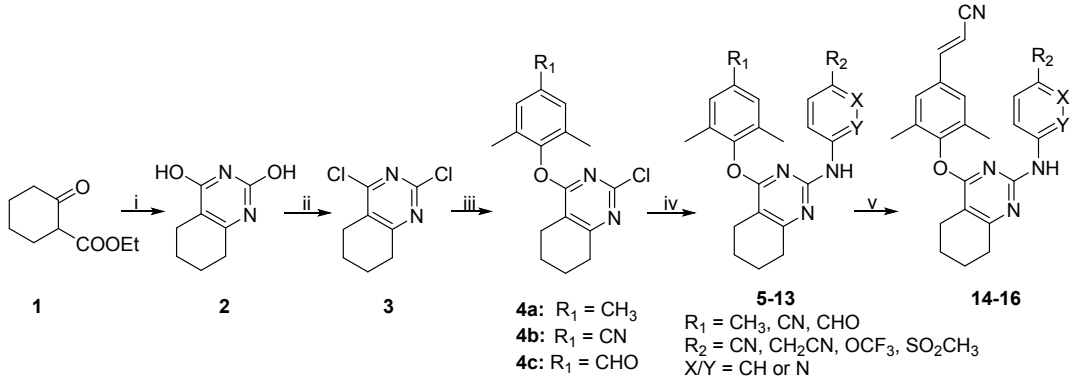

[a]Reagents and conditions: (i) (a): Na, anhydrous EtOH, urea, 80℃, 6 h; (b): water, conc. HCl acidify, pH 3, 0℃. Two steps 66%. (ii) $POCl_3$, 106℃, 5 h, 53%. (iii) 2,4,6-trisubstituted phenols, K_2CO_3, DMF, 60℃, 4-4.5 h, 57%-71%. (iv) substituted anilines or 5-aminopicolinonitrile or 6-aminonicotinonitrile, $Pd_2(dba)_3$, Xantphos, Cs_2CO_3,1,4-dioxane, N_2, reflux, 4-9 h, 12%-76%. (v) $(EtO)_2POCH_2CN$, *t*-BuOK, THF, 0℃ to r.t., 1 h, 45%-64%.

Scheme 2. Synthesis of Target Compounds 20-22[a]

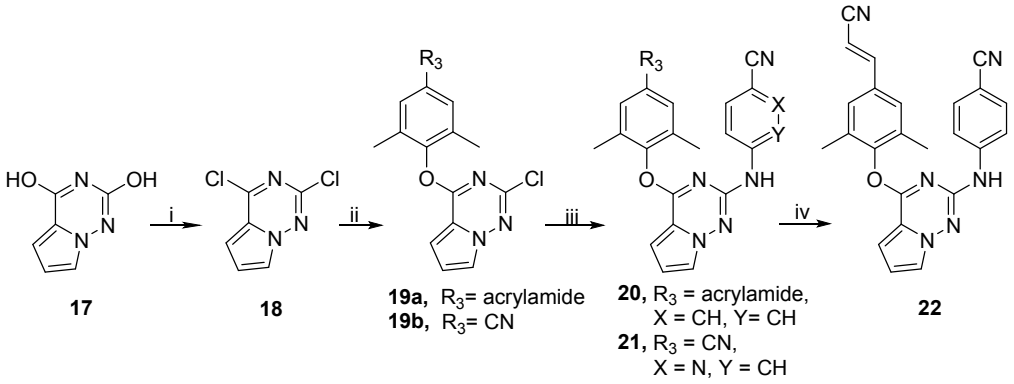

[a]Reagents and conditions: (i) $POCl_3$, DIPEA, 120℃, 24 h, 50%. (ii) 2,4,6-trisubstituted phenols, K_2CO_3, DMF, r.t., 6 h, 27%-66%. (iii) $Pd(OAc)_2$, BINAP, Cs_2CO_3, 1,4-dioxane, N_2, reflux, 8 h, 55%-63%. (iv) **20**, $POCl_3$, 40℃, 5 h, 48%.

Scheme 3. Synthesis of Target Compounds 26-31[a]

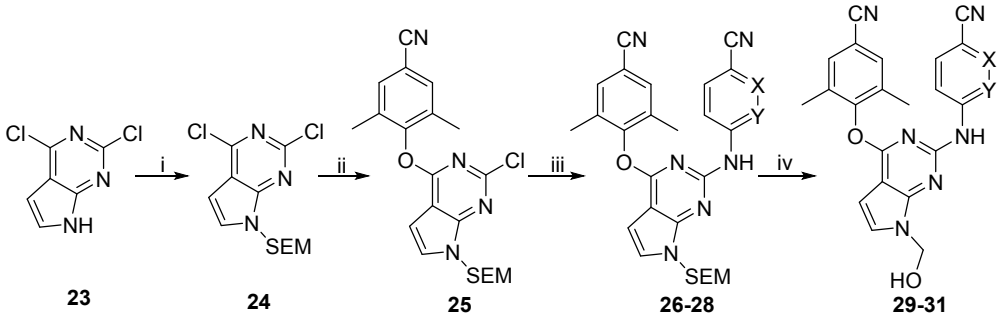

[a]Reagents and conditions: (i) SEM-Cl, NaH, DMF, 0℃ to r.t., 4 h, 80%. (ii) K_2CO_3, DMF, r.t. to 60℃, 3 h, 92%. (iii) 4-aminobenzonitrile or 5-aminopicolinonitrile or 6-aminonicotinonitrile, $Pd_2(dba)_3$, Xantphos, Cs_2CO_3, 1,4-dioxane, N_2, reflux, 4 h, 46%-67%. (iv) TFA, methylene chloride, r.t., 2 h, 45%-100%.

Scheme 4. Synthesis of Target Compound 33[a]

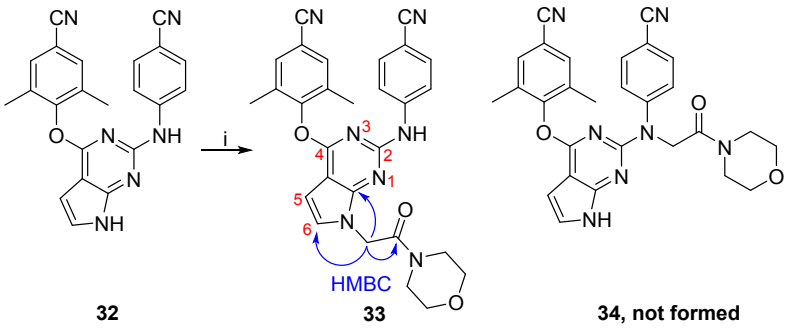

[a]Reagents and conditions: (i) 4-(Chloroacetyl)morpholine, NaH, THF, r.t., 5 h, 36%.

RESULTS AND DISCUSSION

Antiviral and HIV-1 RT Inhibitory Activities and SAR Analysis.

All target compounds were first evaluated for their anti-HIV potency and cytotoxicity using the MTT (3-(4,5-dimethylthiazol-2-yl)-2,5-diphenyltetrazolium bromide) method in MT-4 cells infected with WT HIV-1 strain (III_B) and K103N/Y181C double mutant HIV-1 strain (RES056), as well as HIV-2 strain (ROD).[34] EFV, ETR, RPV and DOR were used as controls. The antiviral evaluation results, interpreted as EC_{50} (anti-HIV potency), CC_{50} (cytotoxicity) and SI (selectivity index, CC_{50}/EC_{50} ratio), are summarized in Table 1-2.

Table 1. Antiviral Potency Against HIV-1 III_B and RES056 Strains and Cytotoxicity of the Target Compounds 5-16 (Series I) in MT-4 Cells.

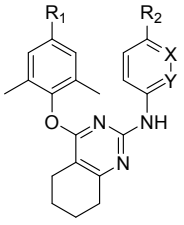

5-16

Compds	R_1	R_2	X	Y	EC_{50} (nM)[a] III_B	EC_{50} (nM)[a] RES056	CC_{50} (μM)[b]	SI[c] III_B	SI[c] RES056	ClogP[d]	Fsp^3
5	CH_3	CN	CH	CH	38.6 ± 22.6	805 ± 160	6.8 ± 1.0	177	8	6.55	0.29
6	CN	CN	CH	CH	10.6 ± 1.6	205 ± 27.9	3.1 ± 0.02	298	15	5.86	0.25
7	CHO	CN	CH	CH	35.1 ± 29.2	1201 ± 44.4	5.9 ± 0.32	169	5	5.89	0.25
8	CN	CN	N	CH	1072 ± 317	> 12612	244 ± 6.8	228	< 19	4.86	0.26
9	CHO	CN	N	CH	35.4 ± 18.7	9213 ± 1381	20.9 ± 3.8	590	2	4.89	0.26
10	CHO	CN	CH	N	234 ± 77.9	≥ 35299	293 ± 10.6	1252	≤ 8	5.00	0.26
11	CN	CH_2CN	CH	CH	11.7 ± 3.3	1022 ± 22.4	4.5 ± 1.3	385	4	6.07	0.28
12	CN	OCF_3	CH	CH	80.6 ± 37.6	> 275,058	> 275	> 3413	X1[e]	7.07	0.29
13	CN	SO_2CH_3	CH	CH	56.7 ± 8.1	> 278,682	> 279	> 4916	X1	4.97	0.29
14	CV[f]	CN	CH	CH	14.0 ± 4.8	68.2 ± 28.7	7.2 ± 5.1	513	105	6.62	0.23
15	CV	CN	N	CH	7.6 ± 3.7	58.8 ± 4.5	8.8 ± 5.1	1155	150	5.61	0.24
16	CV	CH_2CN	CH	CH	17.7 ± 13.0	433 ± 82.8	48.3 ± 13.5	2729	112	6.82	0.26
EFV	-	-	-	-	4.5 ± 0.53	144 ± 25.8	> 6.3	> 1394	> 44	4.53	-
ETR	-	-	-	-	4.8 ± 1.1	47.3 ± 4.5	> 4.6	> 950	> 97	5.03	0.10
RPV	-	-	-	-	1.00 ± 0.27[g]	10.7 ± 7.96[g]	3.98[g]	3989[g]	371[g]	5.46	0.09
DOR	-	-	-	-	13 ± 4[h]	15 ± 6[h]	> 294[h]	> 21940[h]	> 20136[h]	2.08	-

[a] EC_{50}: concentration of compound required to achieve 50% protection of MT-4 cell cultures against HIV-1-induced cytotoxicity, as determined by the MTT method.

[b] CC_{50}: concentration required to reduce the viability of mock-infected cell cultures by 50%, as determined by the MTT method.

[c] SI: selectivity index, the ratio of CC_{50}/EC_{50}.

[d] Calculated using the free online Molinspiration software (http://www.molinspiration.com/).

[e] X1: ≥1 or <1.

[f] CV: cyanovinyl.

[g] Used for comparison. The data were obtained from the same laboratory with the same method (Prof. Christophe Pannecouque, Rega Institute for Medical Research, KU Leuven, Belgium).[35]

[h] Used for comparison. The data were obtained from the same laboratory with the same method (Prof. Christophe Pannecouque, Rega Institute for Medical Research, KU Leuven, Belgium).[36]

As shown in Table 1, except for **8** and **10**, all compounds demonstrated excellent antiretroviral potency against WT HIV-1 strain in the one- to two-digit nanomolar range. Compound **15** turned out to be the most potent inhibitor with an EC_{50} value of 7.6 ± 3.7 nM in this series of compounds, which was lower than that of DOR (EC_{50} = 13 ± 4 nM), while was somehow higher than those of EFV (EC_{50} = 4.5 ± 0.53 nM), ETR (EC_{50} = 4.8 ± 1.1 nM) and RPV (EC_{50} = 1.00 ± 0.27 nM). In the case of K103N/Y181C double mutant HIV-1 strain RES056, two compounds **14** and **15** both featuring a cyanovinyl substituent on the left ring exhibited double-digit nanomolar inhibitory potency with EC_{50} values of 68.2 ± 28.7 nM and 58.8 ± 4.5 nM, respectively. **14** and **15** were about 2.1- and 2.4-fold more potent than EFV (EC_{50} = 144 ± 25.8 nM), comparable with ETR (EC_{50} = 47.3 ± 4.5 nM), while less potent than RPV (EC_{50} = 10.7 ± 7.96 nM) and DOR (EC_{50} = 15 ± 6 nM). Moreover, all compounds were endowed with relatively high SI values toward the WT HIV-1 strain. It is worth noting that all the synthesized compounds had large ClogP values (around or more than 5), which was considered to be partially attributed to the installation of the fused cyclohexyl ring, regardless of the introduction of the nitrogen atom.

The contribution of the R_1 substituent of these new analogues to the antiretroviral potencies was first examined. Comparisons between **5**, **6**, **7**, and **14** clearly indicated that cyano and cyanovinyl groups are more favorable at this position. Meanwhile, this conclusion was somehow contradictory when comparing compounds **8**, **9**, and **15**; Compound **8** with a cyano substituent at R_1 position was the least potent while **15** with a cyanovinyl substituent was the most potent. Additionally, comparing the EC_{50} values of compounds **11** and **16**, we found that the cyano group was more beneficial to the inhibitory potency than the cyanovinyl moiety. On the whole, both of the cyano group and the cyanovinyl moiety at R_1 position seemed to be favorable to anti-HIV activity.

Next, the nature of the R_2 substitution on the right wing was explored. Comparing the potencies of compounds **6**, **11**, **12**, and **13**, or **14** and **16**, it can be concluded that the R_2 substitution roughly contributed to the HIV-1 inhibitory activity in the following order: $CN > CH_2CN > SO_2CH_3 > OCF_3$. The cyano group is still the most preferred substituent at R_2 position, which was in agreement with a previous study.[37]

The influence of introduction of a nitrogen atom onto the right benzene ring was finally investigated. For a nitrogen atom at the *meta* position of the pyridylamine moiety (corresponding to the *NH* group), no distinct features were exhibited in this case, as compound **6** (EC_{50} = 10.6 ± 1.6 nM, R_1 = CN) was much more potent than **8** (EC_{50} = 1072 ± 317 nM, R_1 = CN), while compound **7** (EC_{50} = 35.1 ± 29.2 nM, R_1 = CHO) was equipotent as **9** (EC_{50} = 35.4 ± 18.7 nM, R_1 = CHO) and compound **15**

(EC_{50} = 7.6 ± 3.7 nM, R_1 = CV) was nearly 2-fold more potent than **14** (EC_{50} = 14.0 ± 4.8 nM, R_1 = CV). It was therefore speculated that the influence of the introduction of a nitrogen atom at the *meta* position of the pyridylamine moiety on the anti-HIV-1 (WT) potency might rely on the nature of the R_1 substituent. Moreover, introduction of a nitrogen atom at the *ortho* position of the pyridylamine moiety seemed to be deleterious for the HIV-1 inhibitory effect (**10** *vs* **7**), though this conclusion needed to be further explored since only one pair of compounds was prepared.

Furthermore, by comparisons of **6**, **11**, **12**, and **13**, it can be concluded that both OCF_3 and SO_2CH_3 at R_2 position were beneficial for decreased cytotoxicity. Moreover, it was indicated that introduction of a nitrogen atom at the *meta* position of the pyridylamine moiety was also favorable for lower cytotoxicity (**6** *vs* **8**, **7** *vs* **9**, and **14** *vs* **15**).

Intriguingly, we can see that all the designed compounds had greater Fsp^3 contents, ranging from 0.23 to 0.29, than ETR (0.10) and RPV (0.09) as expected, suggesting that these compounds could be characterized as drug-like molecules. Meanwhile, as mentioned above, the ClogP values of all compounds from series I were pretty large, which may lead to unsatisfactory metabolism stability profiles.[27, 38] Based on the known SARs derived from series I of designed compounds, the cyano group in the right wing was kept, while one nitrogen atom containing five-membered ring, instead of the cyclohexyl ring, was fused with the pyrimidine ring, and hydrophilic hydroxymethyl and *N*-acetylmorpholinyl moieties were further introduced onto the

five-membered ring (series II). We anticipated to identify new anti-HIV-1 inhibitors with maintained or even improved potency as well as decreased hydrophobicities.

It was found that all compounds in series II displayed anti-HIV-1 (WT) potency at nanomolar to submicromolar levels except **28** (Table 2). Four compounds exhibited one-digit nanomolar antiretroviral potency, among which compound **30** featuring a hydroxymethyl moiety acted as the most potent inhibitor (EC_{50} = 1.7 ± 0.35 nM) that was 2.6-, 2.8-, and 7.6-fold more potent than EFV, ETR, and DOR respectively, and comparable with RPV. Additionally, compound **22** suppressed the replication of K103N/Y181C double mutant HIV-1 strain as the most potent one with an EC_{50} value of 61.1 ± 0.52 nM, which was 2.4-fold more potent than EFV (EC_{50} = 144 ± 25.8 nM), while less potent than ETR (EC_{50} = 47.3 ± 4.5 nM), RPV (EC_{50} = 10.7 ± 7.96 nM) and DOR (EC_{50} = 15 ± 6 nM).

As expected, all the hydroxymethyl- and *N*-acetylmorpholinyl-containing compounds possessed smaller ClogP values (less than 5) compared to those compounds in series I. Pairwise comparisons between compounds **26-28** and **29-31** demonstrated that the hydroxymethyl moiety is more favorable for decreased ClogP than the large 2-(trimethylsilyl)ethoxymethyl (SEM) moiety. To cross check if the ClogP values of all the target compounds in the present study were reliable, we also utilized another free online tool (http://molsoft.com/mprop/) to obtain another set of ClogP values (Table S1). Linear regression analysis results indicated that the ClogP values employed should be reliable (R^2 = 0.83, Figure S1).

Detailed SAR conclusions could be derived from these analogues. Comparing to compound **20** with an acrylamide group, compound **22** bearing a cyanovinyl group was three times more potent. Dramatical potency increases were observed against both HIV-1 III_B and RES056 between compound **21** (EC_{50} = 7.0 ± 2.1 nM and 1221 ± 5.6 nM) and compound **8** (EC_{50} = 1072 ± 317 nM and > 12612 nM), suggesting the central core may exert a remarkable impact on the antiviral activity and the pyrrolo[2,1-f][1,2,4]triazine core was preferred. Moreover, the large SEM moiety was found to be detrimental for the anti-HIV-1 potency, since compounds **26-28** exhibited only submicromolar level activity against III_B strain and even lost activity against both III_B and RES056 strains at the highest concentration tested. In contrast, the hydroxymethyl-containing compounds **29-31** displayed significantly elevated antiretroviral activity against III_B. Furthermore, comparisons among compounds **26-28** and among **29-31** led to the conclusion that introduction of nitrogen atom at the *meta* position of the pyridylamine moiety was favorable for HIV-1 inhibitory activity, while introduction of a nitrogen atom at the *ortho* position of the pyridylamine moiety was unfavorable. Compound **33** also demonstrated one-digit nanomolar anti-HIV-1 (III_B) potency, indicating that the *N*-acetylmorpholinyl moiety was tolerant.

It should be noted that the cyanovinyl group bearing compound **22** demonstrated the highest cytotoxicity profile among **20**-**22**. Comparisons between **26** and **27**, or **29** and **30** further confirmed that introduction of a nitrogen atom at the *meta* position of the pyridylamine moiety was favorable for decreased cytotoxicity.

Table 2. Antiviral Potency Against HIV-1 III_B and RES056 Strains and Cytotoxicity of the Target Compounds 20-22, 26-31, and 33 (Series II) in MT-4 Cells.

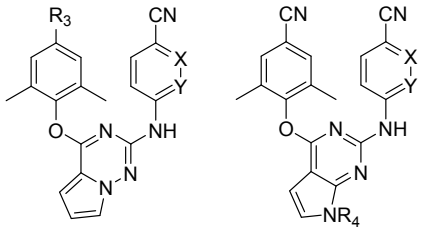

20-22 **26-31, 33**

					EC_{50} (nM)[a]		CC_{50} (μM)[b]	SI[c]		
Compds	**R_3**	**R_4**	**X**	**Y**	**III_B**	**RES056**		**III_B**	**RES056**	**ClogP**
20	acrylamide	-	CH	CH	36.3 ± 24.6	5854 ± 550	57.6 ± 46.1	1588	10	4.75
21	CN	-	N	CH	7.0 ± 2.1	1221 ± 5.6	69.1 ± 34.5	9828	57	4.05
22	CV	-	CH	CH	12.6 ± 4.9	61.1 ± 0.52	5.0 ± 0.92	395	81	5.80
26	-	SEM[d]	CH	CH	820 ± 602	> 2957	3.0 ± 1.1	4	< 1	7.36
27	-	SEM	N	CH	253 ± 4.1	> 117,217	117 ± 8.2	463	< 1	6.36
28	-	SEM	CH	N	> 93,881	> 93,881	93.9 ± 61.3	< 1	< 1	6.46
29	-	CH_2OH	CH	CH	6.1 ± 2.2	128 ± 23.3	0.83 ± 0.29	137	6	4.43
30	-	CH_2OH	N	CH	1.7 ± 0.35	319 ± 119	> 60.8	> 35,039	> 190	3.43
31		CH_2OH	CH	N	46.9 ± 22.7	> 138,298	≥ 138	≥2948	X1[e]	3.53
33	-	CH_2CO-Morp[f]	CH	CH	7.7 ± 0.72	782 ± 39.0	2.3 ± 0.91	297	3	4.27
EFV	-	-	-		4.5 ± 0.53	144 ± 25.8	> 6.3	> 1394	> 44	4.53
ETR	-	-	-	-	4.8 ± 1.1	47.3 ± 4.5	> 4.6	> 950	> 97	5.03
RPV	-	-	-	-	1.00 ± 0.27[g]	10.7 ± 7.96[g]	3.98[g]	3989[g]	371[g]	5.46
DOR	-	-	-	-	13 ± 4[h]	15 ± 6[h]	> 294[h]	> 21940[h]	> 20136[h]	2.08

[a] EC_{50}: concentration of compound required to achieve 50% protection of MT-4 cell cultures against HIV-1-induced cytotoxicity, as determined by the MTT method.

[b] CC_{50}: concentration required to reduce the viability of mock-infected cell cultures by 50%, as determined by the MTT method.

[c] SI: selectivity index, the ratio of CC_{50}/EC_{50}.

[d] SEM: 2-(trimethylsilyl)ethoxymethyl.

[e] X1: ≥1 or <1.

[f] Morp: morpholino.

[g] Used for comparison. The data were obtained from the same laboratory with the same method (Prof. Christophe Pannecouque, Rega Institute for Medical Research, KU Leuven, Belgium).[35]

[h] Used for comparison. The data were obtained from the same laboratory with the same method (Prof. Christophe Pannecouque, Rega Institute for Medical Research, KU Leuven, Belgium).[36]

Based on the promising anti-HIV-1 (WT) results, selected compounds were further evaluated for their inhibitory effects on the E138K and a variety of other NNRTI-resistant HIV-1 strains, including K103N, Y181C, Y188L, L100I, and F227L/V106A. As illustrated in Table 3, most compounds demonstrated moderate to excellent potency in inhibiting replication of the HIV-1 variants. The antiretroviral results against these drug-resistant strains can be summarized as follows:

(1) In terms of the E138K variant, which is the key drug-resistant strain to diarylpyrimidine derivatives, though some compounds did not show activity at the highest tested concentrations, four compounds **6**, **14**, **30**, and **33** showed potent inhibitory activity at two- or single- digit nanomolar levels. Intriguingly, compounds **30** (EC_{50} = 4.9 ± 1.7 nM) and **33** (EC_{50} = 6.8 ± 0.98 nM) were 3.1- and 2.2-fold more potent than ETR (EC_{50} = 15.2 ± 4.9 nM) respectively, and **30** was slightly more active than EFV (EC_{50} = 6.0 ± 0.45 nM).

(2) As for K103N, which is the most prevalent single mutant strain resistant to first-generation NNRTIs, all selected compounds were endowed with low EC_{50} values ranging from 63.7 nM to 1.8 nM, being more potent than EFV (EC_{50} = 89.2 ± 19.5 nM). Among them, **30** possessed 2.2-fold greater activity than ETR (EC_{50} = 3.9 ± 0.32 nM), and **29** (EC_{50} = 3.7 ± 0.69 nM) was as potent as ETR. It was noted that the cyano group at R_1 position was more favorable for anti-HIV-1 (K103N) activity than the cyanovinyl moiety by comparisons between **6** and **14**, or between **11** and **16**.

(3) In case of Y181C, two compounds **22** (EC_{50} = 19.7 ± 8.7 nM) and **30** (EC_{50} = 23.8 ± 5.2 nM) were equipotent with ETR (EC_{50} = 21.3 ± 4.7 nM). We found that introduction of a nitrogen atom at the *meta* position of the pyridylamine moiety was beneficial for HIV-1 inhibitory activity (both Y181C and K103N), by pairwise comparing **14** and **15**, or **29** and **30**.

(4) For Y188L, compound **6** (EC_{50} = 24.5 ± 8.6 nM) exhibited slightly greater activity than ETR (EC_{50} = 27.2 ± 5.4 nM), and **14**, **30**, and **33** possessed two-digit nanomolar inhibitory activity as well; For L100I, compound **22** (EC_{50} = 7.8 ± 0.87 nM) was almost as potent as ETR (EC_{50} = 7.4 ± 0.65 nM), and compounds **6** and **15** showed the same potency with an EC_{50} value of 12.8 nM as the second best ones. In total, seven compounds were more potent than EFV.

(5) Two compounds **6** (EC_{50} = 58.4 ± 0.72 nM) and **14** (EC_{50} = 95.3 ± 4.2 nM) were found to be potent inhibitors against the F227L/V106A variant at two-digit nanomolar

concentration, which were more potent than EFV (EC_{50} = 274 ± 26.9 nM), though less potent than ETR (EC_{50} = 25.7 ± 2.6 nM).

Table 3. Antiviral Potency of Selected Target Compounds against Several HIV-1 Mutant Strains in MT-4 Cells.

Compds	EC_{50} (nM)[a]					
	E138K	K103N	Y181C	Y188L	L100I	F227L/V106A
5	171 ± 5.5	57.0 ± 1.1	232 ± 81.3	191 ± 52.8	96.9 ± 6.1	524 ± 74.9
6	19.0 ± 4.6	7.1 ± 1.8	52.7 ± 11.6	24.5 ± 8.6	12.8 ± 3.8	58.4 ± 0.72
7	146 ± 60.7	63.7 ± 31.6	748 ± 9.2	663 ± 316	492 ± 96.4	2245 ± 357
11	> 4518	9.9 ± 2.2	283 ± 133	> 4518	68.5 ± 25.4	> 4518
14	61.3 ± 3.5	17.0 ± 1.2	40.9 ± 5.9	77.9 ± 0.50	18.0 ± 6.4	95.3 ± 4.2
15	> 8829	7.7 ± 0.17	34.8 ± 21.4	> 8829	12.8 ± 3.0	> 8829
16	> 25785	12.9 ± 0.32	140 ± 71.1	> 25785	49.0 ± 14.4	> 25785
21	> 69114	11.9 ± 2.8	171 ± 89.5	> 69114	204 ± 82.7	> 69114
22	> 41309	4.8 ± 0.87	19.7 ± 8.7	> 41309	7.8 ± 0.87	> 41309
29	> 707	3.7 ± 0.69	31.2 ± 1.7	> 707	20.1 ± 10.2	> 707
30	4.9 ± 1.7	1.8 ± 0.52	23.8 ± 5.2	53.4 ± 15.6	20.1 ± 5.0	102 ± 2.6
33	6.8 ± 0.98	5.9 ± 0.28	148 ± 5.9	56.7 ± 2.8	154 ± 77.2	146 ± 62.4
EFV	6.0 ± 0.45	89.2 ± 19.5	6.0 ± 1.8	244 ± 46.1	51.6 ± 0.0	274 ± 26.9
ETR	15.2 ± 4.9	3.9 ± 0.32	21.3 ± 4.7	27.2 ± 5.4	7.4 ± 0.65	25.7 ± 2.6

[a] EC_{50}: concentration of compound required to achieve 50% protection of MT-4 cell cultures against HIV-1-induced cytotoxicity, as determined by the MTT method.

As expected, none of the synthesized compounds displayed inhibitory activity against the HIV-2 strain (ROD) at subtoxic concentrations (data not shown). In general, the present drug design scenario to target the dual tolerant regions of HIV-1 NNIBP has proven effective with these promising results, yielding several potent lead compounds that were endowed with marked inhibitory activities against WT and NNRTI-resistant HIV-1 strains.

We further tested all the newly synthesized pyridyl-bearing fused bicyclic derivatives for their ability to inhibit recombinant WT HIV-1 RT, with ETR and RPV as reference drugs (Table 4). These compounds displayed HIV-1 RT inhibitory activity in the range of 61 μM - 0.014 μM, and nearly two thirds of them (14/22) showed two-digit nanomolar potency. Compound **21** featuring a pyridyl moiety in the right wing demonstrated the most active RT-inhibitory activity with an IC_{50} value of 0.014 μM in the same magnitude with ETR (0.011 μM) and RPV (0.022 μM). In brief, the results indicated that these inhibitors exhibited antiretroviral activity by inhibiting the HIV-1 RT enzyme, and should be classified as typical HIV-1 NNRTIs.

Table 4. Inhibitory Activity of the Newly Synthesized Compounds Against HIV-1 RT (WT)[a]

Compds	IC_{50} (μM)	Compds	IC_{50} (μM)
5	0.241 ± 0.042	**16**	0.049 ± 0.002
6	0.052 ± 0.009	**20**	0.053 ± 0.002
7	0.055 ± 0.007	**21**	0.014 ± 0.002
8	0.050 ± 0.004	**22**	0.043 ± 0.002

9	0.043 ± 0.000	**26**	0.171 ± 0.007
10	0.058 ± 0.000	**27**	7.40 ± 3.61
11	0.053 ± 0.005	**28**	31 ± 2.58
12	61 ± 5.35	**29**	0.040 ± 0.002
13	0.069 ± 0.003	**30**	0.036 ± 0.000
14	0.119 ± 0.003	**31**	0.047 ± 0.002
15	0.147 ± 0.020	**33**	0.155 ± 0.010
ETR	0.011 ± 0.000[b]	RPV	0.022 ± 0.004

[a] IC_{50}: The RT inhibition assay is performed with the EnzCheck Reverse Transcriptase Assay kit (Molecular Probes, Invitrogen).

[b] Used for comparison. The data was obtained from the same laboratory with the same method (Prof. Christophe Pannecouque, Rega Institute for Medical Research, KU Leuven, Belgium).

In Vitro Metabolic Stability Profiles and Other Drug-Like Properties

To further validate our hypothesis, we selected several compounds including **14, 15, 22, 30** and **33**, and tested their metabolic stability profiles in human liver microsome. As delineated in Table 5, except for **33**, the other compounds exhibited improved metabolic stability and lower intrinsic clearance than those of RPV ($t_{1/2}$ = 12.8 min, $CL_{int(liver)}$ = 97.6 mL/min/kg) and better than those of the three reference drugs. Comparison between **14** ($t_{1/2}$ = 27.4 min) and **15** ($t_{1/2}$ = 26.5 min) suggested that introduction of a nitrogen atom at the *meta* position of the pyridylamine moiety seemed to have marginal influence on metabolic stability. Comparing to **14**, compound **22** ($t_{1/2}$ = 43.3 min) possessed 1.6-fold better metabolic stability, revealing that the installation of the fused five-membered ring (pyrrolyl ring) was preferred over

the cyclohexyl ring. Compound **30** bearing a hydroxymethyl group with the smallest ClogP value (3.43) was 2.7-fold more stable than RPV in human liver microsome. Collectively, the preliminary structure-metabolic stability relationships explored in the present study gave directions for next-step structural modifications to increase metabolic stability profiles of designed small molecules.

Ligand efficiency (LE) has been applied as an important metric to guide lead optimization campaigns in modern drug discovery.[39, 40] Therefore, those five compounds together with compound **6** were assessed for their lipophilic properties (Table 5). Except for **33** (LE = 0.29), all the selected compounds had greater LE values (> 0.3), which were very close to each other. The results demonstrated that our drug design proposal has been fulfilled well, and, certainly, led to compounds with a delicate balance between anti-HIV-1 potency and other drug-like properties.

Table 5. Metabolic Stability, cLogP, LE and LLE Values of Compounds 6, 14, 15, 22, 30, 33 and Controls

Compds	HLM $t_{1/2}$ (min) (R^2)[a]	$CL_{int(liver)}$ (mL/min/kg)[b]	cLogP (< 5)	LE[c] (> 0.3)
6	ND[d]	ND	5.86	0.36
14	27.4 (0.9365)	45.5	6.62	0.34
15	26.5 (0.9781)	47	5.61	0.35
22	43.3 (0.9016)	28.8	5.80	0.35
30	34.2 (0.9725)	36.5	3.43	0.39

33	3.1 (0.9995)	397	4.27	0.29
RPV	12.8 (0.9544)	97.6	5.46	NA
Testosterone	9.9 (0.9361)	125.5	NA[e]	NA
Diclofenac	4.0 (0.9984)	310	NA	NA
Propafenone	5.9 (0.9359)	235.3	NA	NA

[a] R^2 is the corelation coefficient of the linear regression for the determination of kinetic constant.

[b] $CL_{int(liver)}$: intrinsic clearance.

[c] LE: calculated by the formula $-\Delta G/N_{(non\text{-}hydrogen\ atom)}$, where standard free energy change $\Delta G = -RT \ln Kd$, presuming $Kd \approx EC_{50}$; negative logarithm values of potency (pEC_{50}) converted from experimental data against WT HIV-1 (III_B). R is the Gas constant 8.31 $J \cdot K^{-1} \cdot mol^{-1}$, and T is 300 K. $N_{(non\text{-}hydrogen\ atom)}$ is the number of non-hydrogen atoms.

[d] ND: not determined.

[e] NA: not applicable.

Molecular Modeling Studies

Classical molecular dynamics (MD) simulations were carried out to verify the stability of compounds **6**, **15, 21** and **30** into the HIV-1 NNIBP. The WT HIV-1 RT (PDB ID: 6C0J), the E138K variant (PDB code: 6C0L) that confers resistance to diarylpyrimidine derivatives, and the K103N variant (PDB code: 6C0K), all were co-crystallized with our previously reported small-molecule NNRTI **K-5a2**.[41] This compound closely resembles the inhibitors studied here, and was used to examine the binding modes of **6**, **15, 21** and **30** (details about the computational procedure can be found in the Supporting Information). In particular, the analysis of the MD simulations (250 ns) run for the ligand-bound complexes was focused on the potential

effect of the nitrogen atom introduced into the A-ring that targets the tolerant region I as well as on the fused (five- and six- membered) ring with additional hydrophilic groups that fills the tolerant region II. Attention was also paid to the effect of the E138K and K103N mutations, mapping at the tolerant regions of the NNIBP, on the ligand binding. Accordingly, a total of seven systems (RT-**6**, RT-**15**, RT-**21**, RT-**30**, RT_{E138K}-**6**, RT_{E138K}-**30** and RT_{K103N}-**30**) were first studied.

The analysis of the trajectories supported the structural integrity of all the ligand-bound complexes, as noted in the stability of the positional root-mean square deviation (RMSD) profiles determined for the residues that shape the NNRTI binding pocket and the ligand along the MD simulations (Figures S2 and S6). All the ligands adopted a common pose (U shape) in the NNRTI binding site of the WT HIV-1 RT,[18] as noted in the snapshots collected at the end of the MD trajectories for RT bound to **6**, **15, 21** and **30** (Figure 5). As observed in previous studies,[42, 43] the left 2,4,6-trisubstitued moieties in the four compounds remain stably accommodated into a hydrophobic sub-pocket shaped by Y181, Y188, and W229 (Figure 5 A-D). On the opposite site, the right benzonitrile moiety (**6**) or picolinonitrile moiety (**15**, **21**, **30**) was situated in the tolerant region I. It is noteworthy that the picolinonitrile moiety was able to adopt conformations with the N atom pointing to Y318. However, no specific hydrogen-bonding interaction was formed between the N atom with residues in the tolerant region I, which enabled also the adoption of conformations where the N atom was oriented toward the 2,4,6-trisubstitued moiety. On the other hand, the

presence of the five- or six-membered ring fused with the 2-aminopyrimidine (or 1,2,4-triazine-3-amine) unit, as well as the hydroxymethyl group in case of **30**, seemed to be accommodated in the tolerant region II, as noted in the lack of notable local structural distortions in this sub-pocket.

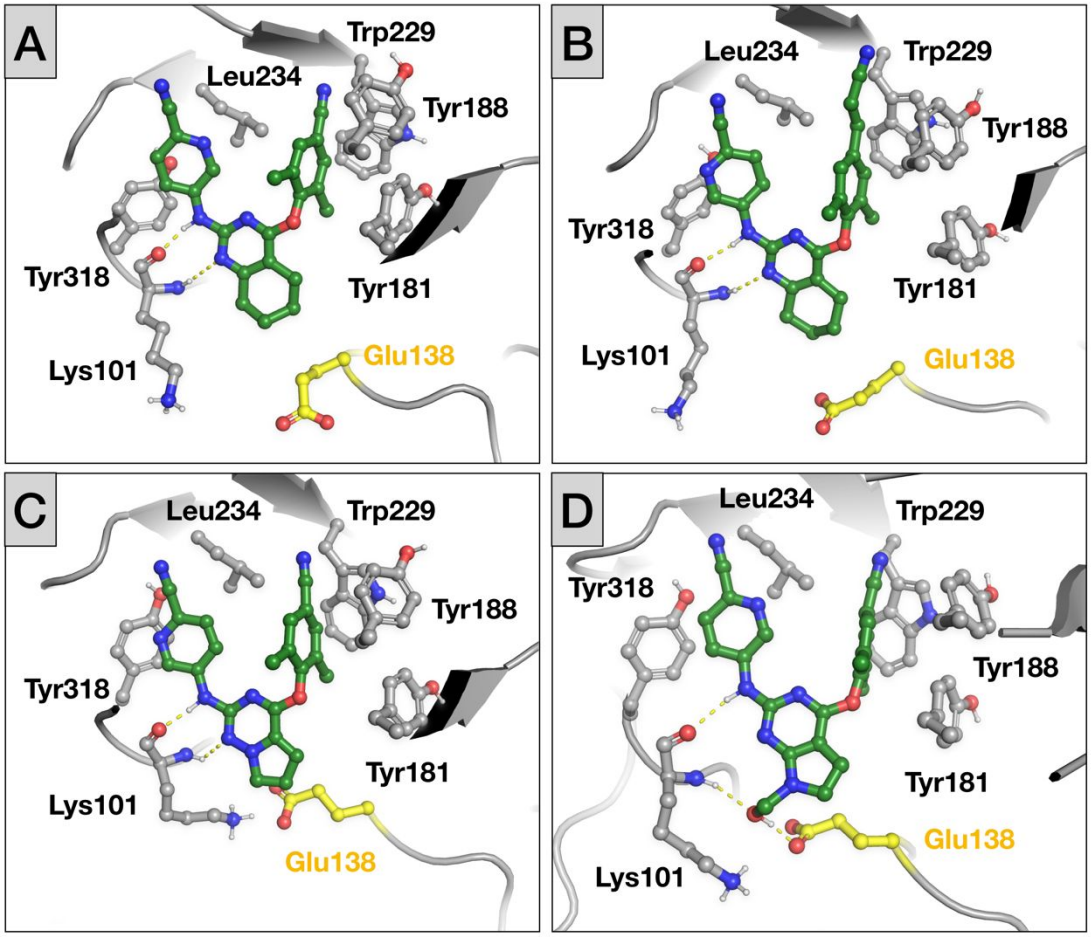

Figure 5. Final complexes for (A) RT-**6**, (B) RT-**15**, (C) RT-**21** and (D) RT-**30** obtained from MD simulation. Selected residues are highlighted as sticks (carbon atoms in grey), and the ligand is shown as green (carbon atoms) sticks. E138 is highlighted with carbon atoms in yellow.

In all cases, stable hydrogen-bonding interactions were formed between the 2-aminopyrimidine ring (1,2,4-triazine-3-amine in case of **21**) of the ligands and the backbone (both *NH* and C=O units) of K101. Thus, the hydrogen bond formed by the *NH* group of the ligands and the carbonyl oxygen of K101 amounts on average to 2.9 ± 0.1 Å in all cases (*d1* in Table S2 and blue profiles in Figure S3). In fact, all the compounds exhibited a similar ability to establish an interaction with the carbonyl oxygen atom, as noted in the similar interaction energies (from -13.2 to -11.6 kcal/mol; Figure S4) obtained from the molecular interaction potential (MIP) maps determined using an oxygen probe (mimicking the carbonyl oxygen). Compounds **6**, **15** and **21** were able to form an additional hydrogen bond between the pyrimidine N (or the pyrrolo[2,1-f][1,2,4]triazine N in case of **21**) and the backbone *NH* of K101. Compared to the hydrogen-bonding interaction mentioned above, this latter interaction involved a larger distance between the pyrimidine and the nitrogen atom of the backbone *NH* of K101 (average value of 3.6 ± 0.2 Å; *d2* in Table S2 and green profiles in Figure S3), which was also reflected in higher interaction energies (from -7.3 to -4.3 kcal/mol; Figure S5) observed from the MIP maps calculated using a hydrogen probe that mimics the amide hydrogen. Although these findings pointed to the relevance of the double hydrogen bonds formed with the backbone of K101 in assisting the proper binding to the WT HIV-1 RT binding pocket, this latter hydrogen bond was weakened in the complex formed with compound **30**, as the distance between the hydrogen-bonded atoms increased up to 4.0 ± 0.2 Å (*d2* in Table S2 and

Figure S3). Meanwhile, this effect can be compensated by the additional hydrogen bond afforded by the hydroxymethyl group of **30**, which was able to establish a simultaneous interaction as hydrogen-bond acceptor with the backbone NH group of K101 (average distance of 3.3 ± 0.3 Å; *d3* in Table S2 and orange profiles in Figure S3) and as hydrogen-bond donor to the carboxylate group of E138 (average distance of 3.6 ± 0.4 Å; *d4* in Table S2 and violet profiles in Figure S3) upon binding to the WT enzyme. Overall, it is reasonable to speculate that the presence of these two additional interactions could contribute to the high inhibitory potency of **30** against the WT HIV-1 strain (EC_{50} = 1.7 ± 0.35 nM).

The final protein-ligand complex for **6** bound to RT_{E138K}, and **30** in the complexes with RT_{E138K} and RT_{K103N} are shown in Figure 6, while the RMSD profiles are reported in Figure S6. No significant effects are produced by the E138K and K103N point mutations on the stability of the binding modes of **6** and **30** into the NNRTI binding site. In particular, the two previously cited hydrogen-bonding interactions involving the ligand and both the C=O (K101) (average distance of 3.0 ± 0.1 Å; *d1* in Table S2 and blue profiles in Figure S7) and NH (K101) (average distance of 3.7 ± 0.2 Å; *d2* in Table S2 and green profiles in Figure S7) units are in fact well preserved during the simulation. The positive contribution to ligand binding given by the hydroxymethyl moiety of **30** at the tolerant region II is maintained in the two mutated variants. Remarkably, although the hydrogen-bonding interaction with the carboxylic unit of E138 was lost due to the E138K mutation, the hydrogen-bond formed with the

NH unit of K101 is well preserved in the RT_{E138K}-**30** complex (Figure 6B; average distance of 3.4 ± 0.4 Å; *d3* in Table S2 and orange profile in Figure S7B), revealing that the mutation at position 138 can influence but do not abolish the interaction profile. On the other hand, the point mutation at position 103 in the RT_{K103N}-**30** complex led to a hydrogen bond interaction between the NH group of the amide moiety of the mutated residue, N103, and the backbone C=O unit of K101 (Figure 6C; average value of 3.1 ± 0.3 Å), which thus reinforced the network of hydrogen bonds formed by the ligand and both the NH and the C=O units of K101 already observed in the WT enzyme (average distances of 3.2 ± 0.2 Å and 3.5 ± 0.2 Å; *d3* and *d4* in Table S2 and orange and violet profiles in Figure S7C). In conjunction with the similar binding mode observed for **6** and **30** in the WT HIV-1 RT, the present results support the similar inhibitory potencies determined against both the WT enzyme and mutated variants (**6**: EC_{50} values of 10.6 ± 1.6 nM and 19.0 ± 4.6 nM for WT RT and RT_{E138K}; **30**: EC_{50} values of 1.7 ± 0.35 nM, 4.9 ± 1.7 nM and 1.8 ± 0.52 nM for WT RT, RT_{E138K} and RT_{K103N}).

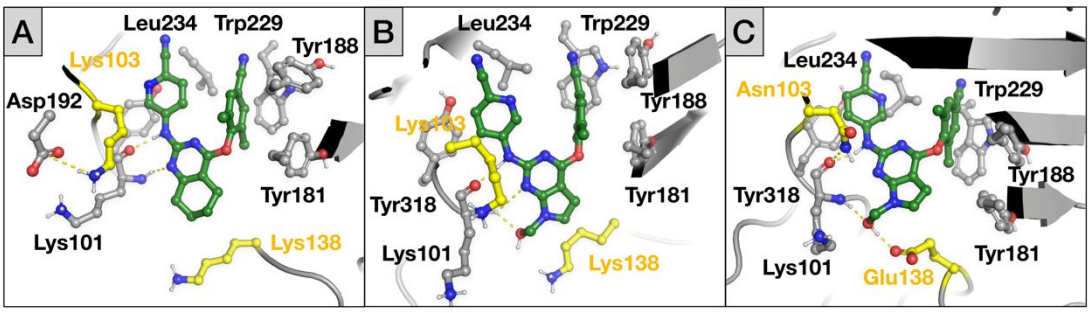

Figure 6. Final complexes for (A) RT_{E138K}-**6**, (B) RT_{E138K}-**30**, and (C) RT_{K103N}-**30** obtained from MD simulations. Selected residues are highlighted as sticks (carbon atoms in grey), and the ligand

is shown as green (carbon atoms) sticks. Residues at position 103 and 138 are highlighted in yellow (carbon atoms).

Another critical point of the allosteric NNRTIs binding site is represented by the hydrophobic area shaped by the aromatic residues Tyr181, Tyr188 and Tpr229. According to the epidemiological data, mutations at position 181 such as the single RT Y181V, Y181C or the double RT K103/Y181C variants, are quite common and responsible for potency reduction of several first-generation NNRTIs.[44] The potential structural implications of the Y181C point mutation on ligand potency is examined for compound **30** in Figure 7. On the basis of previous study,[44] the Y181C mutation is not expected to promote relevant changes in the protein fold with regard to the WT RT according to the comparison of the X-ray structures of the WT (PDB code: 4H4M) and Y181C mutated variant (PDB code: 4RW6). Indeed, superposition of these X-ray structures reveals a close match of the protein backbone (positional root-mean square deviation of 1.4 Å), and the shape of the binding pocket is well preserved. In the simulated WT RT-**30** complex (**Figure 7A**), the trisubstituted phenyl ring is stably accommodated around the aromatic residues Tyr181, Tyr188 and Tpr229. As previously said, stacking interactions (in particular with Tyr181) contribute to stabilize binding of **30**.

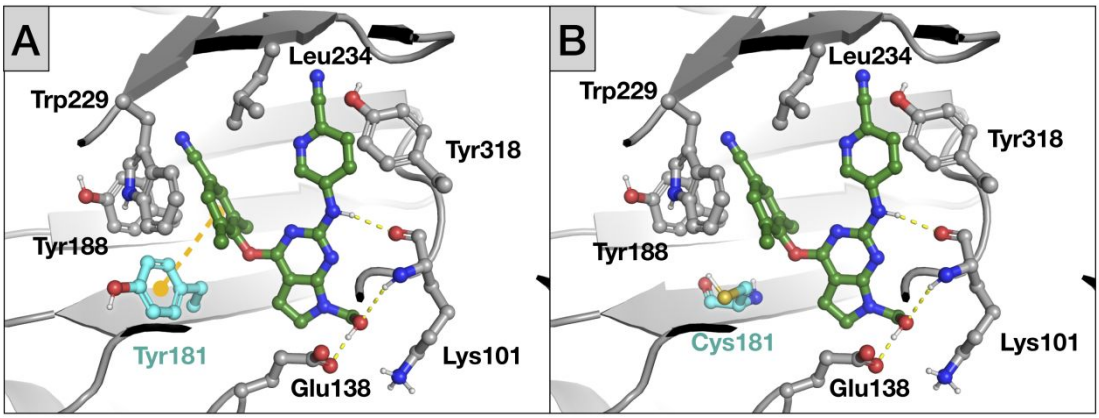

Figure 7. Binding modes of **30** into the NNIBPs of the WT (**A**) and Y181C (**B**) HIV-1 RT. The point mutation was introduced on the WT RT by using the mutagenesis tool of PyMOL. Some key residues shaping the NNIBP are highlighted as grey sticks while ligand is shown as green sticks. The stacking with Tyr181 is also highlighted with a yellow dashed line.

Comparison with the WT RT reveals that the Y181C mutation (**Figure 7B**) would destabilize the binding mode of **30** by partially disrupting the network of protein-ligand hydrophobic interactions. The Y181C mutation would also contribute to slightly enhance volume cavity with a negative impact on the stability of the previously described ligand binding mode (EC_{50} values of 1.7 ± 0.35 nM for WT RT vs. 23.8 ± 5.2 nM for the Y181C RT).

CONCLUSIONS

Based on the X-ray crystallographic analysis and previous SAR studies, we have designed and synthesized two series of pyridyl-bearing fused bicyclic derivatives targeting dual tolerant regions of NNIBP, aiming at identification of potent antiretroviral agents with improved anti-resistance and metabolic stability profiles. Several compounds demonstrated potent inhibitory activities against wild-type HIV-1 strain or multiple NNRTI-resistant strains at low nanomolar levels. The current SAR study revealed that: (1) the cyano group at the 4-position of the right A ring is still preferred. Most interestingly, we found that the introduction of the N atom into the ortho position of the above mentioned cyano group of the A ring moiety is well tolerant, while introduction of the N atom into the meta position of the cyano group is deleterious for anti-HIV-1 activity; (2) It seems that the five-membered fused rings are preferred. More importantly, the hydroxymethyl and *N*-acetylmorpholinyl moieties are favorable for antiretroviral potency, providing possibilities for combating drug resistance from the E138K mutant, a major HIV-1 variant with resistance to the NNRTI drugs ETR and RPV. For instance, compounds **30** and **33** were 3.1- and 2.2-fold more potent than ETR against the E138K mutant HIV-1 strain; (3) the cyano and cyanovinyl groups at the para position of the C ring are favorable, and the cyano group seemed more favorable for anti-HIV-1 (K103N) activity than the cyanovinyl moiety. Furthermore, *in vitro* metabolic stability profiles in human liver microsome of selected compounds were evaluated, and the results indicated that the moieties introduced to target the tolerant region II influenced the metabolic stability. The

molecular modeling studies with representative compounds **6**, **15**, **21**, and **30** further elucidated the binding modes of such compounds in the binding pocket of WT, E138K, K103N or Y181C HIV-1 RTs and furnished a rationale supporting the roles of the introduced moieties in anti-HIV-1 activity.

It should be noted that the latest NNRTI drug doravirine has been reported to have a novel resistance pathway so that it retains in vitro activity against clinically relevant NNRTI viral mutations including K103N, E138K, and Y181C.[45] However, doravirine exhibits inferior antiviral activity against the WT HIV-1 strain.[36] Furthermore, V106A and Y188L have also been selected by doravirine in vitro and in vivo.[46-48] Additionally, the double mutants F227L/V106A is associated with substantial resistance to doravirine.[45, 49] Meanwhile, some compounds in the present study were found to be potent inhibitors against WT, Y188L and F227L/V106A HIV-1 strains, which showed great promise to combat HIV-1 comparing to doravirine. Taken together, the present study has offered several promising lead compounds, which warrant further optimization campaign to afford more potent anti-HIV-1 agents.

EXPERIMENTAL SECTION

Chemistry

All melting points (Mp) were determined on a micromelting point apparatus and are uncorrected. Mass spectra (MS) were performed on a LC Autosampler Device:

Standard G1313A instrument by electrospray ionization. 1D ^{1}H NMR and ^{13}C NMR spectra were obtained on a Bruker AV-400 spectrometer (Bruker BioSpin, Fällanden, Switzerland) in the indicated solvent DMSO-d_6. 2D NMR spectra of compound **33** were recorded on a BrukerAvance DRX-600 spectrometer (^{1}H NMR: 600 MHz, ^{13}C NMR: 150 MHz) in DMSO-d_6. Chemical shifts were expressed in δ units (ppm), with or without TMS (tetramethylsilane) as an internal standard, and J values were reported in hertz (Hz). TLC was performed on Silica Gel GF254. Spots were visualized with iodine vapor and/or by irradiation with UV light (λ 254 nm). Flash column chromatography was carried out on columns packed with silica gel 60 (200–300 mesh). Solvents were of reagent grade and, if needed, were purified and dried by standard methods. The key reagents were purchased from commercial suppliers and no further purified when used. Rotary evaporators were served in concentration of the reaction solutions under reduced pressure. Analysis of the sample purity was performed on a waters e2695 HPLC (high performance liquid chromatography) system using a waters 2998 detector and GOLD-C18 analytical column (5 μm; 250 mm × 4.6 mm). HPLC eluent conditions: acetonitrile/water, varied as follows: (A) from 0 to 15 min, acetonitrile increased from 40% to 90% gradually; from 15 to 16 min, acetonitrile decreased from 90% to 40% gradually; from 16 to 18 min, acetonitrile was kept at 40%; (B) from 0 to 15 min, acetonitrile increased from 60% to 90% gradually; from 15 to 16 min, acetonitrile decreased from 90% to 60% gradually; from 16 to 18 min, acetonitrile was kept at 60%. Flow rate,

1.0 mL/min; UV detection, from 200 to 600 nm; temperature, ambient; injection volume, 2 μL. The purity of representative final compounds was checked by HPLC and all was > 95%.

*5,6,7,8-tetrahydroquinazoline-2,4-diol (**2**).* Sodium (0.54 g, 23.50 mmol) was first disssolved in anhydrous ethanol (25 mL), and then urea (1.06 g, 17.63 mmol) was added. The resulting mixture was stirred for 5 min at room temperature. Ethyl 2-oxocyclohexane-1-carboxylate **1** (2.00 g, 11.75 mmol) was dropwised added into the solution. The reaction mixture was heated at 80℃ for 6 h. The excess sovlent was removed under reduced pressure. The residue was then redissolved in water and washed with ethyl acetate (3 × 30 mL). The aqueous layer was adjusted to pH 3 by addition of concentrated hydrochloric acid at 0℃ (ice-water bath). The precipitate was filtered, washed with water and dried in vacuum to provide **2** as a light yellow solid. Yield: 66%. Decomposed at 284.8℃. ESI-MS: *m/z* 167.5 $[M + H]^+$, 189.5 $[M + Na]^+$, $C_8H_{10}N_2O_2$ (166.07).

*2,4-dichloro-5,6,7,8-tetrahydroquinazoline (**3**).* Compound **2** (1.00 g, 6.02 mmol) was suspended in $POCl_3$ (10 mL), and then the mixture was heated at 106℃ for 5 h. After cooling to room temperature, the reaction mixture was poured into ice-water. The precipitate was filtered, washed with water for three times and dried in vacuum to give the crude product **3** as a pale brown solid, which could be used in the next step without further purification. Yield: 53%. Mp: 70.2-71.3℃. ESI-MS: *m/z* 203.2 $[M + H]^+$, $C_8H_8Cl_2N_2$ (202.01).

*General Procedure for the Preparation of Intermediates **4(a-c)***. The corresponding commercially available 2,4,6-trisubstituted phenol (2.46 mmol) and potassium carbonate (0.68 g, 4.92 mmol) were mixed in distilled DMF (6 mL) and the mixture was stirred at room temperature for 10 min. Intermediate **3** (0.50 g, 2.46 mmol) was added, and then the resulting mixture was heated at 60℃ until the completion monitored by TLC (4 - 4.5 h). After cooling to room temperature, water (15 mL) was added. The precipitate was filtered, washed with water and dried in vacuum to give the pure key intermediates **4(a-c)**.

*2-Chloro-4-(mesityloxy)-5,6,7,8-tetrahydroquinazoline (**4a**)*. White solid. Yield: 65%. ESI-MS: *m/z* 303.4 $[M + H]^+$, $C_{17}H_{19}ClN_2O$ (302.12).

*4-((2-chloro-5,6,7,8-tetrahydroquinazolin-4-yl)oxy)-3,5-dimethylbenzonitrile (**4b**)*. White solid. Yield: 71%. Mp: 187.2-188.8℃. ESI-MS: *m/z* 314.4 $[M + H]^+$, $C_{17}H_{16}ClN_3O$ (313.10).

*4-((2-chloro-5,6,7,8-tetrahydroquinazolin-4-yl)oxy)-3,5-dimethylbenzaldehyde (**4c**)*. White solid. Yield: 57%. Mp: 138.1-139.2℃. ESI-MS: *m/z* 317.4 $[M + H]^+$, 339.5 $[M + Na]^+$, $C_{17}H_{17}ClN_2O_2$ (316.10).

*General Procedure for the Preparation of Target Compounds **5-13***. The intermediate **4a** or **4b** or **4c** (1 equiv), substituted aniline or 5-aminopicolinonitrile or 6-aminonicotinonitrile (1 equiv), cesium carbonate (1.5 equiv), $Pd_2(dba)_3$ (1.5% equiv or 7.5% equiv), and xantphos (1.5% equiv or 7.5% equiv) were mixed in 1,4-dioxane (8 mL). The resulting mixture was heated to reflux under N_2 protection for 4-9 h. After cooling to room temperature, the mixture was filtered through celite and the filtrate was evaporated to remove excess solvent. The residue was purified by column chromatography and further recrystallized in anhydrous methanol to provide pure

target compounds among **5-13**. Or, acetonitrile was added to the residue mentioned above and the mixture was filtered. The solid was redissolved in dichloromethane (5 mL) and the solution was filtered again. The filtrate was evaporated to remove dichloromethane, and the residue was suspended in anhydrous methanol and filtered to supply pure target compounds among **5-13**.

*4-((4-(Mesityloxy)-5,6,7,8-tetrahydroquinazolin-2-yl)amino)benzonitrile (**5**).* White solid. Yield: 22%. Mp: 202.1-203.0°C. ^{1}H NMR (400 MHz, DMSO-d_6) δ: 9.86 (s, 1H, NH), 7.51 (d, J = 8.80 Hz, 2H, Ph-H), 7.37 (d, J = 8.80 Hz, 2H, Ph-H), 7.01 (s, 2H, Ph-H), 2.71-2.70 (m, 4H, cyclohexane-H), 2.33 (s, 3H, CH_3), 2.01 (s, 6H, CH_3 × 2), 1.83 (brs, 4H, cyclohexane-H). ^{13}C NMR (100 MHz, DMSO-d_6) δ: 167.77, 166.74, 156.70, 148.28, 145.65, 134.82, 132.89 (Ph-C × 2), 130.25 (Ph-C × 2), 129.52 (Ph-C × 2), 120.05, 118.07 (Ph-C × 2), 107.61, 101.99, 31.85, 22.31, 22.20, 21.53, 20.84 (CH_3), 16.44 (CH_3 × 2). ESI-MS: *m/z* 385.4 $[M + H]^+$, $C_{24}H_{24}N_4O$ (384.20).

*4-((2-((4-Cyanophenyl)amino)-5,6,7,8-tetrahydroquinazolin-4-yl)oxy)-3,5-dimethyl benzonitrile (**6**).* White solid. Yield: 61%. Mp: 231.6-232.2°C. ^{1}H NMR (400 MHz, DMSO-d_6) δ: 9.93 (s, 1H, NH), 7.77 (s, 2H, Ph-H), 7.47-7.41 (m, 4H, Ph-H), 2.73-2.72 (m, 4H, cyclohexane-H), 2.10 (s, 6H, CH_3 × 2), 1.84 (brs, 4H, cyclohexane-H). ^{13}C NMR (100 MHz, DMSO-d_6) δ: 168.59, 166.06, 156.56, 154.49, 145.42, 133.13 (Ph-C × 2), 133.04 (Ph-C × 2), 132.94 (Ph-C × 2), 119.96, 119.12, 118.01 (Ph-C × 2), 108.79, 107.61, 102.27, 31.92, 22.24, 22.11, 21.42, 16.20 (CH_3 × 2). ESI-MS: *m/z* 396.3 $[M + H]^+$, 413.5 $[M + NH_4]^+$, $C_{24}H_{21}N_5O$ (395.17). HPLC purity: 100%.

4-((4-(4-Formyl-2,6-dimethylphenoxy)-5,6,7,8-tetrahydroquinazolin-2-yl)amino)benzonitrile (7). White solid. Yield: 62%. Mp: 214.6-216.2°C. ^{1}H NMR (400 MHz, DMSO-d_6) δ: 10.03 (s, 1H, CHO), 9.92 (s, 1H, NH), 7.80 (s, 2H, Ph-H), 7.44 (d, J = 8.80 Hz, 2H, Ph-H), 7.34 (d, J = 8.88 Hz, 2H, Ph-H), 2.73 (brs, 4H, cyclohexane-H), 2.15 (s, 6H, CH_3 × 2), 1.85 (brs, 4H, cyclohexane-H). ^{13}C NMR (100 MHz, DMSO-d_6) δ: 192.91 (CHO), 168.47, 166.23, 156.61, 155.54, 145.44, 134.21, 132.94 (Ph-C × 2), 132.30 (Ph-C × 2), 130.45 (Ph-C × 2), 119.96, 117.97 (Ph-C × 2), 107.59, 102.19, 31.91, 22.26, 22.14, 21.46, 16.47 (CH_3 × 2). ESI-MS: *m/z* 399.3 $[M + H]^+$, 416.5 $[M + NH_4]^+$, 421.4 $[M + Na]^+$, $C_{24}H_{22}N_4O_2$ (398.17).

*5-((4-(4-Cyano-2,6-dimethylphenoxy)-5,6,7,8-tetrahydroquinazolin-2-yl)amino)picolinonitrile (**8**)*. White solid. Yield: 46%. Decomposed at 268.7°C. ^{1}H NMR (400 MHz, DMSO-d_6) δ: 10.11 (s, 1H, NH), 8.67 (d, J = 2.24 Hz, 1H, pyridine-H), 7.89 (d, J = 7.64 Hz, 1H, pyridine-H), 7.76 (s, 2H, Ph-H), 7.63 (d, J = 8.72 Hz, 1H, pyridine-H), 2.74 (t, J = 5.68 Hz, 4H, cyclohexane-H), 2.11 (s, 6H, CH_3 × 2), 1.85 (brs, 4H, cyclohexane-H). ^{13}C NMR (100 MHz, DMSO-d_6) δ: 168.64, 166.15, 156.32, 154.24, 141.48, 141.07, 133.08 (Ph-C × 2), 133.03 (Ph-C × 2), 129.33, 123.54, 123.37, 119.09, 118.62, 108.93, 108.40, 31.93, 22.18, 22.05, 21.45, 16.20 (CH_3 × 2). ESI-MS: *m/z* 397.4 $[M + H]^+$, 414.4 $[M + NH_4]^+$, $C_{23}H_{20}N_6O$ (396.17).

*5-((4-(4-Formyl-2,6-dimethylphenoxy)-5,6,7,8-tetrahydroquinazolin-2-yl)amino)picolinonitrile (**9**)*. White solid. Yield: 76%. Mp: 224.5-226.1°C. ^{1}H NMR (400 MHz, DMSO-d_6) δ: 10.11 (s, 1H, CHO), 10.01 (s, 1H, NH), 8.65 (d, J = 2.32 Hz, 1H,

pyridine-H), 7.86 (d, J = 7.36 Hz, 1H, pyridine-H), 7.79 (s, 2H, Ph-H), 7.54 (d, J = 8.72 Hz, 1H, pyridine-H), 2.76-2.74 (m, 4H, cyclohexane-H), 2.15 (s, 6H, CH_3 × 2), 1.86 (brs, 4H, cyclohexane-H). ^{13}C NMR (100 MHz, DMSO-d_6) δ: 192.84, 168.54, 166.32, 156.38, 155.29, 141.52, 141.10, 134.24, 132.21 (Ph-C × 2), 130.50 (Ph-C × 2), 129.33, 123.39, 123.29, 118.61, 108.40, 31.92, 22.20, 22.08, 21.49, 16.46 (CH_3 × 2). ESI-MS: *m/z* 400.3 $[M + H]^+$, $C_{23}H_{21}N_5O_2$ (399.17).

*6-((4-(4-Formyl-2,6-dimethylphenoxy)-5,6,7,8-tetrahydroquinazolin-2-yl)amino)nicotinonitrile (**10**).* White solid. Yield: 67%. Mp: 264.4-265.7°C. ^{1}H NMR (400 MHz, DMSO-d_6) δ: 10.32 (s, 1H, CHO), 10.02 (s, 1H, NH), 8.56 (d, J = 1.80 Hz, 1H, pyridine-H), 7.79 (s, 2H, Ph-H), 7.58 (dd, J_1 = 8.96 Hz, J_2 = 2.28 Hz, 1H, pyridine-H),7.44 (d, J = 8.96 Hz, 1H, pyridine -H), 2.75 (brs, 4H, cyclohexane-H), 2.15 (s, 6H, CH_3 × 2), 1.86 (brs, 4H, cyclohexane-H). ^{13}C NMR (100 MHz, DMSO-d_6) δ: 192.90, 168.79, 166.13, 156.00, 155.58, 155.34, 152.40, 140.66, 134.25, 132.27 (Ph-C × 2), 130.45 (Ph-C × 2), 118.23, 111.15, 108.84, 100.77, 31.94, 22.21, 22.02, 21.48, 16.45 (CH_3 × 2). ESI-MS: *m/z* 400.3 $[M + H]^+$, $C_{23}H_{21}N_5O_2$ (399.17).

*4-((2-((4-(Cyanomethyl)phenyl)amino)-5,6,7,8-tetrahydroquinazolin-4-yl)oxy)-3,5-dimethylbenzonitrile (**11**).* White solid. Yield: 44%. Mp: 192.8-193.4 °C. ^{1}H NMR (400 MHz, DMSO-d_6) δ: 9.44 (s, 1H, NH), 7.75 (s, 2H, Ph-H), 7.29 (d, J = 8.32 Hz, 2H, Ph-H), 6.96 (d, J = 8.56 Hz, 2H, Ph-H), 3.86 (s, 2H, CH_2), 2.70 (brs, 4H, cyclohexane-H), 2.11 (s, 6H, CH_3 × 2) , 1.83 (brs, 4H, cyclohexane-H). ^{13}C NMR (100 MHz, DMSO-d_6) δ: 168.33, 166.05, 157.17, 154.63, 140.60, 133.18 (Ph-C × 2),

132.86 (Ph-C × 2), 128.33 (Ph-C × 2), 123.37, 119.86, 119.10, 118.43 (Ph-C × 2), 108.63, 106.05, 31.93, 22.35, 22.26, 22.13, 21.41, 16.23 (CH_3 × 2). ESI-MS: m/z 410.5 $[M + H]^+$, 427.5 $[M + NH_4]^+$, $C_{25}H_{23}N_5O$ (409.19).

*3,5-Dimethyl-4-((2-((4-(trifluoromethoxy)phenyl)amino)-5,6,7,8-tetrahydroquinazolin-4-yl)oxy)benzonitrile (**12**).* White solid. Yield: 51%. Mp: 206.5-207.9°C. ^{1}H NMR (400 MHz, DMSO-d_6) δ: 9.57 (s, 1H, NH), 7.76 (s, 2H, Ph-H),7.35 (d, J = 8.84 Hz, 2H, Ph-H), 6.96 (d, J = 8.72 Hz, 2H, Ph-H), 2.70 (brs, 4H, cyclohexane-H), 2.10 (s, 6H, CH_3 × 2), 1.83 (brs, 4H, cyclohexane-H). ^{13}C NMR (100 MHz, DMSO-d_6) δ: 168.46, 166.06, 156.96, 154.64, 142.14, 142.13, 140.37, 133.18 (Ph-C × 2), 132.93 (Ph-C × 2), 121.90, 121.28 (Ph-C × 2), 119.37, 119.21 (Ph-C × 2), 119.03, 108.63, 106.42, 31.94, 22.32, 22.21, 21.38, 16.19 (CH_3 × 2). ESI-MS: *m/z* 455.4 $[M + H]^+$, $C_{24}H_{21}F_3N_4O_2$ (454.16).

*3,5-Dimethyl-4-((2-((4-(methylsulfonyl)phenyl)amino)-5,6,7,8-tetrahydroquinazolin-4-yl)oxy)benzonitrile (**13**).* White solid. Yield: 12%. Decomposed at 228.2°C. ^{1}H NMR (400 MHz, DMSO-d_6) δ: 9.99 (s, 1H, NH), 7.79 (s, 2H, Ph-H), 7.53-7.46 (m, 4H, Ph-H), 3.09 (s, 3H, SO_2CH_3), 2.74-2.72 (m, 4H, cyclohexane-H), 2.11 (s, 6H, CH_3 × 2), 1.90-1.79 (m, 4H, cyclohexane-H). ^{13}C NMR (100 MHz, DMSO-d_6) δ: 168.27, 166.18, 156.45, 154.47, 145.59, 133.16 (Ph-C × 2), 133.00 (Ph-C × 2), 132.35, 128.03 (Ph-C × 2), 119.05, 117.66 (Ph-C × 2), 108.79, 107.57, 44.46 (SO_2CH_3), 31.73, 22.18, 22.08, 21.39, 16.20 (CH_3 × 2). ESI-MS: *m/z* 449.5 $[M + H]^+$, 466.4 $[M + NH_4]^+$, $C_{24}H_{24}N_4O_3S$ (448.16).

*General Procedure for the Preparation of Target Compounds **14-16***. Diethyl cyanomethylphosphonate (1.5 equiv) was dissolved in 3 mL of THF, followed by the addition of potassium *tert*-butoxide (1.5 equiv). The resulting mixture was stirred at 0℃ for 30 min. The aldehyde containing compound **7** or **9** (0.12 g, 1 equiv) dissolved in 2 mL of THF was dropwise added to the solution, and the reaction mixture was stirred at room temperature for 1 h. The excess solvent was removed, and water was added to the residue. After filtration, the precipitate was suspended in 5 mL of methanol in sonicator and the mixture was filtered. The solid was washed with methanol and further dried in vacuum to supply target compound **14** or **15**.

Following the same procedure to prepare target compounds **5-13**, intermediate **4c** was reacted with 2-(4-aminophenyl)acetonitrile to provide an aldehyde containing intermediate, which was used through the Wittig-Horner reaction (following the same protocol to generate target compounds **14** and **15**) to offer target compound **16**.

*(E)-4-((4-(4-(2-Cyanovinyl)-2,6-dimethylphenoxy)-5,6,7,8-tetrahydroquinazolin-2-yl)amino)benzonitrile (**14**)*. White solid. Yield: 64%. Mp: 242.0-243.2°C. ^{1}H NMR (400 MHz, DMSO-d_6) δ: 9.90 (s, 1H, NH), 7.68 (d, J = 16.68 Hz, 1H, CH=), 7.54 (s, 2H, Ph-H), 7.47 (d, J = 8.84 Hz, 2H, Ph-H), 7.36 (d, J = 8.88 Hz, 2H, Ph-H), 6.48 (d, J = 16.72 Hz, 1H, CH=), 2.73-2.72 (m, 4H, cyclohexane-H), 2.07 (s, 6H, CH_3 × 2), 1.84 (brs, 4H, cyclohexane-H). ^{13}C NMR (100 MHz, DMSO-d_6) δ: 168.27, 166.44, 156.63, 152.83, 150.58, 145.51, 132.94 (Ph-C × 2), 131.74 (Ph-C × 2), 131.69, 129.54, 128.61 (Ph-C × 2), 119.99, 119.41, 118.03 (Ph-C × 2), 102.14, 96.71, 31.90, 22.27,

22.16, 21.48, 16.49 (CH_3 × 2). ESI-MS: *m/z* 422.4 $[M + H]^+$, 439.5 $[M + NH_4]^+$, $C_{26}H_{23}N_5O$ (421.19).

*(E)-5-((4-(4-(2-Cyanovinyl)-2,6-dimethylphenoxy)-5,6,7,8-tetrahydroquinazolin-2-yl)amino)picolinonitrile (**15**).* White solid. Yield: 45%. Decomposed at 195.8°C. ^{1}H NMR (400 MHz, DMSO-d_6) δ: 10.10 (s, 1H, NH), 8.68 (s, 1H, pyridine-H), 7.92 (d, J = 7.52 Hz, 1H, pyridine-H), 7.79-7.53 (m, 3H, pyridine-H, Ph-H), 7.66 (d, J = 16.56 Hz, 1H, CH=), 7.45 (d, J = 16.68 Hz, 1H, CH=), 2.75 (brs, 4H, cyclohexane-H), 2.08 (s, 6H, CH_3 × 2), 1.85 (brs, 4H, cyclohexane-H). ^{13}C NMR (100 MHz, DMSO-d_6) δ: 168.31, 166.52, 156.40, 152.57, 150.54, 141.58, 141.16, 131.77, 131.64 (Ph-C × 2), 129.29, 128.66 (Ph-C × 2), 123.45, 123.25, 119.40, 118.64, 108.43, 96.81, 31.91, 22.21, 22.10, 21.51, 16.49 (CH_3 × 2). ESI-MS: *m/z* 423.4 $[M + H]^+$, 440.5 $[M + NH_4]^+$, $C_{25}H_{22}N_6O$ (422.19). HPLC purity: 95.09%.

*(E)-3-(4-((2-((4-(Cyanomethyl)phenyl)amino)-5,6,7,8-tetrahydroquinazolin-4-yl)oxy)-3,5-dimethylphenyl)acrylonitrile (**16**).* White solid. Yield: 63%. Decomposed at 146.3°C. ^{1}H NMR (400 MHz, DMSO-d_6) δ: 9.44 (s, 1H, NH), 7.64 (d, J = 16.68 Hz, 1H, CH=), 7.53 (s, 2H, Ph-H), 7.28 (d, J = 8.36 Hz, 2H, Ph-H), 6.90 (d, J = 8.56 Hz, 2H, Ph-H), 6.45 (d, J = 16.68 Hz, 1H, CH=), 3.84 (s, 2H, CH_2), 2.69 (brs, 4H, cyclohexane-H), 2.08 (s, 6H, CH_3 × 2), 1.83 (brs, 4H, cyclohexane-H). ^{13}C NMR (100 MHz, DMSO-d_6) δ: 167.67, 166.51, 157.02, 152.93, 150.44, 140.49, 131.74 (Ph-C × 2), 131.60, 128.51 (Ph-C × 2), 128.30 (Ph-C × 2), 123.35, 119.83, 119.41, 118.56

(Ph-C × 2), 106.14, 96.75, 31.74, 22.32, 22.26, 22.13, 21.43, 16.52 (CH_3 × 2). ESI-MS: *m/z* 436.5 $[M + H]^+$, $C_{27}H_{25}N_5O$ (435.21).

*2,4-Dichloropyrrolo[2,1-f][1,2,4]triazine (**18**).* The starting material pyrrolo[2,1-f][1,2,4]triazine-2,4-diol **17** (0.19 g, 1.26 mmol) was mixed with $POCl_3$ (2 mL) and *N,N*-diisopropylethylamine (2 mL), and then the mixture was heated at 120℃ for 24 h. After cooling to room temperature, the reaction mixture was poured into ice-water. The mixture was extracted with ethyl acetate (30 mL × 3). The organic phases were combined, washed with brine, dried over anhydrous Na_2SO_4, filtered and concentrated. The residue was further purified by column chromatograph and recrystallized in ethanol to give compound **18** as a yellow solid. Yield: 50%. Mp: 87.5-88.0℃. $C_6H_3Cl_2N_3$ (186.97).

*General Procedure for the Preparation of Intermediates **19a** and **19b**.* 2,4-Dichloropyrrolo[2,1-f][1,2,4]triazine **18** (0.20 g, 1.07 mmol), (*E*)-3-(4-hydroxy-3,5-dimethylphenyl)acrylamide or 4-hydroxy-3,5-dimethylbenzonitrile (1.07 mmol) and potassium carbonate (0.15 g, 1.07 mmol) were mixed in distilled DMF (7 mL) and the resulting mixture was stirred at room temperature for 6 h until completion. Water (100 mL) was added. The mixture was extracted with ethyl acetate (40 mL × 3). The organic layers were combined, washed with brine, dried over anhydrous Na_2SO_4, filtered and concentrated. The residue was recrystallized in ethanol to provide intermediate **19a**. Or, when the reaction was completed, water (20 mL) was added to the reaction mixture. The

precipitate was collected by filtration, washed with water and dried in vacuum to give intermediate **19b**.

(E)-3-(4-((2-Chloropyrrolo[2,1-f][1,2,4]triazin-4-yl)oxy)-3,5-dimethylphenyl)acryl amide (**19a**). White solid. Yield: 27 %. Decomposed at 271.5℃. ESI-MS: *m/z* 343.4 $[M + H]^+$, 365.3 $[M + Na]^+$, $C_{17}H_{15}ClN_4O_2$ (342.09).

*4-((2-Chloropyrrolo[2,1-f][1,2,4]triazin-4-yl)oxy)-3,5-dimethylbenzonitrile (**19b**).* Creamy-white solid. Yield: 66 %. Decomposed at 234.0℃. ESI-MS: *m/z* 299.5 $[M + H]^+$, 321.4 $[M + Na]^+$, $C_{15}H_{11}ClN_4O$ (298.06).

*Preparation of Target Compounds **20-22***. The intermediate **19a** (0.25 g, 0.73 mmol), 4-aminobenzonitrile (0.095 g, 0.80 mmol), cesium carbonate (0.48 g, 1.46 mmol), $Pd(OAc)_2$ (0.033 g, 0.15 mmol), and BINAP (0.18 g, 0.29 mmol) were mixed in 1,4-dioxane (10 mL). The resulting mixture was heated to reflux under N_2 protection for 8 h. After cooling to room temperature, the mixture was filtered through celite and the filtrate was evaporated to remove excess solvent. The residue was purified by column chromatography and further recrystallized in anhydrous methanol to provide target compound **20**.

The intermediate **19b** (0.10 g, 0.34 mmol), 5-aminopicolinonitrile (0.044 g, 0.37 mmol), cesium carbonate (0.48 g, 1.46 mmol), $Pd(OAc)_2$ (0.033 g, 0.15 mmol), and BINAP (0.18 g, 0.29 mmol) were mixed in 1,4-dioxane (6 mL). The resulting mixture was heated to reflux under N_2 protection for 8 h. After cooling to room temperature, the mixture was filtered through celite and the filtrate was evaporated to remove excess solvent. The residue was purified by column chromatography and further recrystallized in anhydrous methanol to provide target compound **21**.

Compound **20** (0.07 g, 0.16 mmol) was dissolved in $POCl_3$ (2 mL) and the mixture was stirred at 40℃ for 5 h. After cooling to room temperature, the reaction mixture was poured into ice-water. The mixture was extracted with ethyl acetate (20 mL × 3). The organic phases were combined, washed with brine, dried over anhydrous Na_2SO_4, filtered and concentrated. The residue was recrystallized in ethanol to furnish target compound **22**.

*(E)-3-(4-((2-((4-Cyanophenyl)amino)pyrrolo[2,1-f][1,2,4]triazin-4-yl)oxy)-3,5-dimethylphenyl)acrylamide (**20**)*. White solid. Yield: 55%. Mp: 285.2-286.1°C. ^{1}H NMR (400 MHz, DMSO-d_6) δ: 9.65 (s, 1H, NH), 7.93 (s, 1H, pyrrole-H), 7.82 (d, J = 8.72 Hz, 2H, Ph-H), 7.63 (d, J = 8.68 Hz, 2H, Ph-H), 7.52 (brs, 1H, $CONH_2$), 7.44-7.40 (m, 3H, Ph-H, CH=), 7.13 (brs, 1H, $CONH_2$), 7.01 (d, J = 3.48 Hz, 1H, pyrrole-H), 6.79 (d, J_1 = 4.16 Hz, J_2 = 2.48 Hz, 1H, pyrrole-H), 6.62 (d, J = 15.92 Hz, 1H, CH=), 2.16 (s, 6H, CH_3 × 2). ^{13}C NMR (100 MHz, DMSO-d_6) δ: 167.11, 160.46, 152.17, 149.98, 145.09, 138.82, 133.44, 133.30 (Ph-C × 2), 131.44 (Ph-C × 2), 128.51 (Ph-C × 2), 123.05, 121.17, 120.00, 118.54 (Ph-C × 2), 112.30, 111.76, 103.53, 102.63, 16.52 (CH_3 × 2). ESI-MS: *m/z* 425.4 $[M + H]^+$, 442.5 $[M + NH_4]^+$, $C_{24}H_{20}N_6O_2$ (424.16).

*5-((4-(4-Cyano-2,6-dimethylphenoxy)pyrrolo[2,1-f][1,2,4]triazin-2-yl)amino)picolinonitrile (**21**)*. White solid. Yield: 63%. Mp: 256.7-258.1°C. ^{1}H NMR (400 MHz, DMSO-d_6) δ: 9.89 (s, 1H, NH), 8.90 (d, J = 2.44 Hz, 1H, pyridine-H), 8.28 (dd, J_1 = 8.72 Hz, J_2 = 2.60 Hz, 1H, pyridine-H), 8.01 (dd, J_1 = 2.44 Hz, J_2 = 1.52 Hz, 1H, pyrrole-H), 7.87 (d, J = 8.68 Hz, 1H, pyridine-H), 7.79 (s, 2H, Ph-H), 7.08 (dd, J_1 = 4.52 Hz, J_2 = 1.48 Hz, 1H, pyrrole-H), 6.84 (dd, J_1 = 4.52 Hz, J_2 = 2.52 Hz, 1H, pyrrole-H), 2.19 (s, 6H, CH_3 × 2). ^{13}C NMR (100 MHz, DMSO-d_6) δ: 160.09, 152.75, 151.75, 141.86, 140.68, 133.25 (Ph-C × 2), 133.13 (Ph-C × 2), 129.70, 124.19, 123.69,

121.66, 118.91, 118.63, 112.71, 111.56, 109.63, 103.91, 16.20 (CH_3 × 2). ESI-MS: *m/z* 382.5 $[M + H]^+$, 399.3 $[M + NH_4]^+$, $C_{21}H_{15}N_7O$ (381.13).

*(E)-4-((4-(4-(2-Cyanovinyl)-2,6-dimethylphenoxy)pyrrolo[2,1-f][1,2,4]triazin-2-yl) amino)benzonitrile (**22**).* White solid. Yield: 48%. Decomposed at 221.0°C. ^{1}H NMR (400 MHz, DMSO-d_6) δ: 9.66 (s, 1H, NH), 7.95-7.94 (m, 1H, pyrrole-H), 7.81 (d, J = 8.84 Hz, 2H, Ph-H), 7.65 (d, J = 16.88 Hz, 1H, CH=), 7.63 (d, J = 8.72 Hz, 2H, Ph-H), 7.54 (s, 2H, Ph-H), 7.03 (dd, J_1 = 4.44 Hz, J_2 = 1.28 Hz, 1H, pyrrole-H), 6.81-6.79 (m, 1H, pyrrole-H), 6.48 (d, J = 16.72 Hz, 1H, CH=), 2.16 (s, 6H, CH_3 × 2). ^{13}C NMR (100 MHz, DMSO-d_6) δ: 160.31, 152.10, 151.17, 150.34, 145.05, 133.31 (Ph-C × 2), 132.30, 131.72 (Ph-C × 2), 128.80 (Ph-C × 2), 121.25, 120.01, 119.33, 118.53 (Ph-C×2), 112.36, 111.67, 103.57, 102.65, 97.22, 16.49 (CH_3 × 2). ESI-MS: *m/z* 407.5 $[M + H]^+$, 424.4 $[M + NH_4]^+$, $C_{24}H_{18}N_6O$ (406.15). HPLC purity: 100%.

Intermediates **24** and **25** and target compound **26** were prepared as reported in our previous studies.[33, 50]

*General Procedure for the Preparation of Target Compounds **27** and **28**.* The intermediate **25** (0.40 g, 0.94 mmol), 5-aminopicolinonitrile or 6-aminonicotinonitrile (0.94 mmol), cesium carbonate (0.456 g, 1.4 mmol), $Pd_2(dba)_3$ (13 mg, 0.014 mmol), and xantphos (8 mg, 0.014 mmol) were mixed in 1,4-dioxane (10 mL). The resulting mixture was heated to reflux under N_2 protection for 4 h. After cooling to room temperature, the mixture was filtered through celite and the filtrate was concentrated. The residue was purified by column chromatography and further recrystallized in anhydrous ethanol to give target compound **27** or **28**.

*5-((4-(4-Cyano-2,6-dimethylphenoxy)-7-((2-(trimethylsilyl)ethoxy)methyl)-7H-pyrr olo[2,3-d]pyrimidin-2-yl)amino)picolinonitrile (**27**).* White solid. Yield: 52%. Mp:

208.2-210.0°C. ^{1}H NMR (400 MHz, DMSO-d_6) δ: 10.25 (s, 1H, NH), 9.02 (d, J = 2.32 Hz, 1H, pyridine-H), 8.29 (dd, J_1 = 8.52 Hz, J_2 = 1.36 Hz, 1H, pyridine-H), 7.93 (s, 2H, OPh-H), 7.85 (d, J = 8.72 Hz, 1H, pyridine-H), 7.60 (d, J = 3.64 Hz, 1H, pyrrole-H), 6.72 (d, J = 3.64 Hz, 1H, pyrrole-H), 5.72 (s, 2H, NCH_2), 3.71 (t, J = 8.16 Hz, 2H, OCH_2), 2.28 (s, 6H, CH_3 × 2), 0.98 (t, J = 8.16 Hz, 2H, $SiCH_2$), 0.00 (s, 9H, $SiCH_3$ × 3). ^{13}C NMR (100 MHz, DMSO-d_6) δ: 161.74, 155.37, 154.90, 154.59, 142.26, 141.86, 133.80 (Ph-C × 4), 130.02, 127.96, 124.29, 123.81, 119.65, 119.29, 109.71, 100.23, 99.94, 73.80, 66.66, 18.14, 16.84 (CH_3 × 2), -0.50 ($SiCH_3$ × 3). ESI-MS: *m/z* 512.5 $[M + H]^+$, 529.4 $[M + NH_4]^+$, 534.2 $[M + Na]^+$, $C_{27}H_{29}N_7O_2Si$ (511.22).

*6-((4-(4-Cyano-2,6-dimethylphenoxy)-7-((2-(trimethylsilyl)ethoxy)methyl)-7H-pyrrolo[2,3-d]pyrimidin-2-yl)amino)nicotinonitrile (**28**).* White solid. Yield: 46%. Mp: 211.2-212.3°C. ^{1}H NMR (400 MHz, DMSO-d_6) δ: 10.49 (s, 1H, NH), 8.76 (s, 1H, pyridine-H), 8.03-7.92 (m, 4H, pyridine-H, Ph-H), 7.61 (d, J = 0.64 Hz, 1H, pyrrole-H), 6.68 (d, J = 0.60 Hz, 1H, pyrrole-H), 5.71 (s, 2H, NCH_2), 3.69 (t, J = 7.80 Hz, 2H, OCH_2), 2.27 (s, 6H, CH_3 × 2), 0.96 (t, J = 7.68 Hz, 2H, $SiCH_2$), 0.00 (s, 9H, CH_3 × 3). ^{13}C NMR (100 MHz, DMSO-d_6) δ: 161.52, 156.75, 155.37, 154.64, 153.93, 153.01, 141.36, 133.83 (Ph-C × 2), 133.72 (Ph-C × 2), 128.23, 119.65, 118.90, 111.97, 109.63, 101.16, 100.42, 99.84, 73.66, 66.64, 18.09, 16.80 (CH_3 × 2), -0.50 ($SiCH_3$ × 3). ESI-MS: *m/z* 512.5 $[M + H]^+$, 529.3 $[M + NH_4]^+$, 534.3 $[M + Na]^+$, $C_{27}H_{29}N_7O_2Si$ (511.22).

Target compound **29** was prepared from compound **26** as reported in our previous study.[50]

*General Procedure for the Preparation of Target Compounds **30** and **31***. To a solution of **27** or **28** (0.20 g, 0.39 mmol) in dichloromethane (3 mL) was added 1 mL of trifluoroacetic acid, and then the mixture was stirred at room temperature for 2 h. The excess solvent was removed under reduced pressure, then dichloromethane was added repeatedly and evaporated. Finally, the residue was purified by column chromatography and further recrystallized in anhydrous methanol to provide target compound **30** or **31**.

*5-((4-(4-Cyano-2,6-dimethylphenoxy)-7-(hydroxymethyl)-7H-pyrrolo[2,3-d]pyrimidin-2-yl)amino)picolinonitrile (**30**).* White solid. Yield: 52%. Mp: 218.4-219.5°C. ^{1}H NMR (400 MHz, DMSO-d_6) δ: 10.15 (s, 1H, NH), 8.87 (d, J = 2.08 Hz, 1H, pyridine-H), 8.16 (d, J = 8.44 Hz, 1H, pyridine-H), 7.83 (s, 2H, OPh-H), 7.73 (d, J = 8.72 Hz, 1H, pyridine-H), 7.43 (d, J = 3.64 Hz, 1H, pyrrole-H), 6.60 (d, J = 3.56 Hz, 1H, pyrrole-H), 5.60 (d, J = 3.12 Hz, 2H, CH_2), 2.18 (s, 6H, CH_3 × 2). ^{13}C NMR (100 MHz, DMSO-d_6) δ: 161.02, 154.12, 154.05, 153.91, 141.59, 141.35, 133.24 (Ph-C × 2), 133.18 (Ph-C × 2), 129.42, 126.67, 123.50, 123.08, 119.08, 118.75, 109.09, 99.64, 98.99, 67.34, 16.26 (CH_3 × 2). ESI-MS: *m/z* 412.4 $[M + H]^+$, 429.4 $[M + NH_4]^+$, 434.5 $[M + Na]^+$, $C_{22}H_{17}N_7O_2$ (411.14). HPLC purity: 97.48%.

*6-((4-(4-Cyano-2,6-dimethylphenoxy)-7-(hydroxymethyl)-7H-pyrrolo[2,3-d]pyrimidin-2-yl)amino)nicotinonitrile (**31**).* White solid. Yield: 45%. Decomposed at 328.0°C. ^{1}H NMR (400 MHz, DMSO-d_6) δ: 10.37 (s, 1H, NH), 8.66 (s, 1H, pyridine-H), 7.87-7.83 (m, 4H, pyridine-H, Ph-H), 7.45 (d, J = 3.64 Hz, 1H, pyrrole-H), 6.57 (d, J = 3.56 Hz, 1H, pyrrole-H), 5.60 (d, J = 3.12 Hz, 2H, CH_2), 2.18 (s, 6H, CH_3 × 2). ^{13}C NMR (100 MHz, DMSO-d_6) δ: 160.83, 156.24, 154.14, 153.92, 153.16, 152.43, 140.75, 133.31 (Ph-C × 2), 133.16 (Ph-C × 2), 126.99, 119.11, 118.39, 111.30, 109.05,

100.52, 99.89, 98.95, 67.24, 16.26 (CH_3 × 2). ESI-MS: *m/z* 412.6 $[M + H]^+$, 429.6 $[M + NH_4]^+$, 434.6 $[M + Na]^+$, $C_{22}H_{17}N_7O_2$ (411.14).

*Preparation of 4-((2-((4-cyanophenyl)amino)-7-(2-morpholino-2-oxoethyl)-7H-pyrrolo[2,3-d]pyrimidin-4-yl)oxy)-3,5-dimethylbenzonitrile (**33**).* Well-prepared compound **32**[33] (0.10 g, 0.26 mmol) was dissolved in tetrahydrofuran (5 mL) and NaH (60% in oil, 0.013 g, 0.32 mmol) was added, and the mixture was stirred at room temperature for 10 min. 4-(Chloroacetyl)morpholine (41 μL, 0.32 mmol) was added to the solution, and then the reaction mixture was stirred at room temperature for an additional 4 h. The solvent was removed under reduced pressure, then water was added and the mixture was filtered. The precipitate was further recrystallized in anhydrous methanol to offer the target compound **33** as a white solid. Yield: 36%. Mp: 234.1-235.9°C. ^{1}H NMR (400 MHz, DMSO-d_6) δ: 9.87 (s, 1H, NH), 7.84 (s, 2H, OPh-H), 7.65 (d, J = 8.80 Hz, 2H, CN-Ph-H), 7.50 (d, J = 8.88 Hz, 2H, CN-Ph-H), 7.27 (d, J = 3.60 Hz, 1H, pyrrole-H), 6.56 (d, 1H, J = 3.60 Hz, pyrrole-H), 5.19 (s, 2H, CH_2), 3.74-3.64 (m, 6H, morpholine-H), 3.52-3.51 (m, 2H, morpholine-H), 2.18 (s, 6H, CH_3 × 2). ^{13}C NMR (100 MHz, DMSO-d_6) δ: 166.06, 160.88, 154.84, 154.30, 154.19, 145.76, 133.35 (Ph-C × 2), 133.15 (Ph-C × 2), 132.93 (Ph-C × 2), 128.22, 120.10, 119.11, 118.03 (Ph-C × 2), 108.94, 101.93, 98.97, 98.10, 66.55, 66.52, 46.17, 45.18, 42.37, 16.31 (CH_3 × 2). ESI-MS: *m/z* 508.4 $[M + H]^+$, 525.4 $[M + NH_4]^+$, $C_{28}H_{25}N_7O_3$ (507.20). HPLC purity: 100%.

ASSOCIATED CONTENT

Supporting Information

The Supporting Information is available free of charge on the ACS Publications website. In vitro anti-HIV assays in MT-4 cells, WT HIV-1 RT inhibition assays, metabolic stability assays in human liver microsome, molecular modeling, Tables S1-S2, Figures S1-S7, and ^{1}H-NMR, ^{13}C-NMR and ESI-MS spectra for the target compounds (PDF).

Molecular formula strings (CSV).

AUTHOR INFORMATION

§ Present address: Department of Medicinal Chemistry, School of Pharmacy, Virginia Commonwealth University, 800 E Leigh Street, Richmond, VA 23298, United States.

Corresponding Authors

*P.Z.: e-mail, zhanpeng1982@sdu.edu.cn; phone, 086-531-88382005;

*X.L.: e-mail, xinyongl@sdu.edu.cn; phone, 086-531-88380270.

Notes

The authors declare no conflict of interest.

ACKNOWLEDGMENT

The financial support from the National Natural Science Foundation of China (NSFC Nos. 81973181, 81903453), Key Project of NSFC for International Cooperation (No. 81420108027), the National Key Projects of New Drugs R&D (No. 2019ZX09301-126), Key research and development project of Shandong Province (Nos. 2017CXGC1401, 2019JZZY021011), Science Foundation for Outstanding Young Scholars of Shandong Province (ZR2020JQ31), the Taishan Scholar Program at Shandong Province, Foreign cultural and educational experts Project (GXL20200015001), the Spanish Ministerio de Economía y Competitividad

(SAF2017-88107-R, MDM-2017-0767; AEI/FEDER UE), Generalitat de Catalunya (2017SGR1746) and Consorci de Serveis Universitaris de Catalunya (Molecular Recognition project), and KU Leuven (GOA 10/014) is gratefully acknowledged. We thank K. Erven, K. Uyttersprot and C. Heens for technical assistance with the biological assays.

ABBREVIATIONS

CC_{50}, 50% cytotoxicity concentration; ^{13}C NMR, carbon nuclear magnetic resonance; CV, cyanovinyl; CYP, cytochrome P450; DEPT, distortionless enhancement by polarization transfer; DOR, doravirine; EC_{50}, 50% effective concentration; EFV, efavirenz; ETR, etravirine; Fsp^3, fraction of sp^3 carbon atoms; HAART, highly active antiretroviral therapy; HIV, human immunodeficiency virus; HMBC, heteronuclear multiple bond correlation; ^1H NMR, proton nuclear magnetic resonance; HPLC, high performance liquid chromatography; HSQC, heteronuclear single quantum coherence; IC_{50}, 50% inhibition concentration; LE, ligand efficiency; MD, molecular dynamics; MIP, molecular interaction potential; Mp, melting points; MS, mass spectra; MTT, 3-(4,5-dimethyl-2-thiazolyl)-2,5-diphenyl-2-H-tetrazolium bromide; NNIBP, non-nucleoside reverse transcriptase inhibitor binding pocket; NNRTIs, non-nucleoside reverse transcriptase inhibitors; NRTIs, nucleoside reverse transcriptase inhibitors; NVP, nevirapine; PDB, protein data bank; RMSD, root-mean-square deviation; RPV, rilpivirine; RT, reverse transcriptase; SARs, structure-activity relationships; SEM, 2-(trimethylsilyl)ethoxymethyl; SI, selectivity index; TMS, tetramethylsilane; WT, wild-type.

REFERENCES

1. De Clercq, E. Fifty Years in Search of Selective Antiviral Drugs. *J. Med. Chem.* **2019,** 62, 7322-7339.

2. Gu, S.-X.; Zhu, Y.-Y.; Wang, C.; Wang, H.-F.; Liu, G.-Y.; Cao, S.; Huang, L. Recent Discoveries in HIV-1 Reverse Transcriptase Inhibitors. *Curr. Opin. Pharmacol.* **2020,** 54, 166-172.

3. Zhan, P.; Chen, X.; Li, D.; Fang, Z.; De Clercq, E.; Liu, X. HIV-1 NNRTIs: Structural Diversity, Pharmacophore Similarity, and Implications for Drug Design. *Med. Res. Rev.* **2013,** 33 Suppl 1, E1-72.

4. De Clercq, E. Milestones in the Discovery of Antiviral Agents: Nucleosides and Nucleotides. *Acta Pharmaceutica Sinica B* **2012,** 2, 535-548.

5. De Clercq, E.; Li, G. Approved Antiviral Drugs over the Past 50 Years. *Clin. Microbiol. Rev.* **2016,** 29, 695-747.

6. Zhan, P.; Pannecouque, C.; De Clercq, E.; Liu, X. Anti-HIV Drug Discovery and Development: Current Innovations and Future Trends. *J. Med. Chem.* **2016,** 59, 2849-2878.

7. De Corte, B. L. From 4,5,6,7-Tetrahydro-5-methylimidazo[4,5,1-jk](1,4)benzodiazepin-2(1H)-one (TIBO) to Etravirine (TMC125): Fifteen Years of Research on Non-Nucleoside Inhibitors of HIV-1 Reverse Transcriptase. *J. Med. Chem.* **2005,** 48, 1689-1696.

8. Janssen, P. A. J.; Lewi, P. J.; Arnold, E.; Daeyaert, F.; de Jonge, M.; Heeres, J.; Koymans, L.; Vinkers, M.; Guillemont, J.; Pasquier, E.; Kukla, M.; Ludovici, D.; Andries, K.; de Béthune, M.-P.; Pauwels, R.; Das, K.; Clark, A. D.; Frenkel, Y. V.; Hughes, S. H.; Medaer, B.; De Knaep, F.; Bohets, H.; De Clerck, F.; Lampo, A.; Williams, P.; Stoffels, P. In Search of a Novel Anti-HIV Drug: Multidisciplinary Coordination in the Discovery of 4-[[4-[[4-[(1E)-2-Cyanoethenyl]-2,6-dimethylphenyl]amino]-2-pyrimidinyl]amino]benzonitrile (R278474, Rilpivirine). *J. Med. Chem.* **2005,** 48, 1901-1909.

9. Gu, S.-X.; Lu, H.-H.; Liu, G.-Y.; Ju, X.-L.; Zhu, Y.-Y. Advances in Diarylpyrimidines and Related Analogues as HIV-1 Nonnucleoside Reverse Transcriptase Inhibitors. *Eur. J. Med. Chem.* **2018,** 158, 371-392.

10. Sun, L. Q.; Zhu, L.; Qian, K.; Qin, B.; Huang, L.; Chen, C. H.; Lee, K. H.; Xie, L. Design, Synthesis, and Preclinical Evaluations of Novel 4-Substituted 1,5-Diarylanilines as Potent HIV-1 Non-nucleoside Reverse Transcriptase Inhibitor (NNRTI) Drug Candidates. *J. Med. Chem.* **2012,** 55, 7219-7229.

11. Tian, Y.; Liu, Z.; Liu, J.; Huang, B.; Kang, D.; Zhang, H.; De Clercq, E.; Daelemans, D.; Pannecouque, C.; Lee, K.-H.; Chen, C.-H.; Zhan, P.; Liu, X. Targeting the Entrance Channel of NNIBP: Discovery of Diarylnicotinamide 1,4-Disubstituted 1,2,3-Triazoles as Novel HIV-1 NNRTIs with High Potency against Wild-type and E138K Mutant Virus. *Eur. J. Med. Chem.* **2018,** 151, 339-350.

12. Lansdon, E. B.; Brendza, K. M.; Hung, M.; Wang, R.; Mukund, S.; Jin, D.; Birkus, G.; Kutty, N.; Liu, X. Crystal Structures of HIV-1 Reverse Transcriptase with Etravirine (TMC125) and Rilpivirine (TMC278): Implications for Drug Design. *J. Med. Chem.* **2010,** 53, 4295-4299.

13. Tian, X.; Qin, B.; Wu, Z.; Wang, X.; Lu, H.; Morris-Natschke, S. L.; Chen, C. H.; Jiang, S.; Lee, K.-H.; Xie, L. Design, Synthesis, and Evaluation of Diarylpyridines and Diarylanilines as Potent Non-nucleoside HIV-1 Reverse Transcriptase Inhibitors. *J. Med. Chem.* **2010,** 53, 8287-8297.

14. Liu, N.; Wei, L.; Huang, L.; Yu, F.; Zheng, W.; Qin, B.; Zhu, D.-Q.; Morris-Natschke, S. L.; Jiang, S.; Chen, C.-H.; Lee, K.-H.; Xie, L. Novel HIV-1 Non-nucleoside Reverse Transcriptase Inhibitor Agents: Optimization of Diarylanilines with High Potency against Wild-Type and Rilpivirine-Resistant E138K Mutant Virus. *J. Med. Chem.* **2016,** 59, 3689-3704.

15. Huang, B.; Zhou, Z.; Kang, D.; Li, W.; Chen, Z.; Zhan, P.; Liu, X. Novel Diaryltriazines with a Picolinonitrile Moiety as Potent HIV-1 RT Inhibitors: a Patent Evaluation of WO2016059647(A2). *Expert Opin. Ther. Pat.* **2017,** 27, 9-15.

16. Pennington, L. D.; Moustakas, D. T. The Necessary Nitrogen Atom: A Versatile High-Impact Design Element for Multiparameter Optimization. *J. Med. Chem.* **2017,** 60, 3552-3579.

17. Huang, B.; Kang, D.; Yang, J.; Zhan, P.; Liu, X. Novel Diarylpyrimidines and Diaryltriazines as Potent HIV-1 NNRTIs with Dramatically Improved Solubility: a Patent Evaluation of US20140378443A1. *Expert Opin. Ther. Pat.* **2016,** 26, 281-289.

18. Huang, B.; Chen, W.; Zhao, T.; Li, Z.; Jiang, X.; Ginex, T.; Vílchez, D.; Luque, F. J.; Kang, D.; Gao, P.; Zhang, J.; Tian, Y.; Daelemans, D.; De Clercq, E.; Pannecouque, C.; Zhan, P.; Liu, X. Exploiting the Tolerant Region I of the Non-Nucleoside Reverse Transcriptase Inhibitor (NNRTI) Binding Pocket: Discovery of Potent Diarylpyrimidine-Typed HIV-1 NNRTIs against Wild-Type and E138K Mutant Virus with Significantly Improved Water Solubility and Favorable Safety Profiles. *J. Med. Chem.* **2019,** 62, 2083-2098.

19. Gu, S.-X.; Xiao, T.; Zhu, Y.-Y.; Liu, G.-Y.; Chen, F.-E. Recent Progress in HIV-1 Inhibitors Targeting the Entrance Channel of HIV-1 Non-nucleoside Reverse Transcriptase Inhibitor Binding Pocket. *Eur. J. Med. Chem.* **2019,** 174, 277-291.

20. Ekkati, A. R.; Bollini, M.; Domaoal, R. A.; Spasov, K. A.; Anderson, K. S.; Jorgensen, W. L. Discovery of Dimeric Inhibitors by Extension into the Entrance Channel of HIV-1 Reverse Transcriptase. *Bioorg. Med. Chem. Lett.* **2012,** 22, 1565-1568.

21. Jiang, X.; Huang, B.; Olotu, F. A.; Li, J.; Kang, D.; Wang, Z.; De Clercq, E.; Soliman, M. E. S.; Pannecouque, C.; Liu, X.; Zhan, P. Exploiting the Tolerant Region I of the Non-nucleoside Reverse Transcriptase Inhibitor (NNRTI) Binding Pocket. Part 2: Discovery of Diarylpyrimidine Derivatives as Potent HIV-1 NNRTIs with

High Fsp3 Values and Favorable Drug-like Properties. *Eur. J. Med. Chem.* **2021,** 213, 113051.

22. Bollini, M.; Cisneros, J. A.; Spasov, K. A.; Anderson, K. S.; Jorgensen, W. L. Optimization of Diarylazines as Anti-HIV Agents with Dramatically Enhanced Solubility. *Bioorg. Med. Chem. Lett.* **2013,** 23, 5213-5216.

23. Kang, D.; Ruiz, F. X.; Feng, D.; Pilch, A.; Zhao, T.; Wei, F.; Wang, Z.; Sun, Y.; Fang, Z.; De Clercq, E.; Pannecouque, C.; Arnold, E.; Liu, X.; Zhan, P. Discovery and Characterization of Fluorine-Substituted Diarylpyrimidine Derivatives as Novel HIV-1 NNRTIs with Highly Improved Resistance Profiles and Low Activity for the hERG Ion Channel. *J. Med. Chem.* **2020,** 63, 1298-1312.

24. Sun, Y.; Kang, D.; Da, F.; Zhang, T.; Li, P.; Zhang, B.; De Clercq, E.; Pannecouque, C.; Zhan, P.; Liu, X. Identification of Novel Potent HIV-1 Inhibitors by Exploiting the Tolerant Regions of the NNRTIs Binding Pocket. *Eur. J. Med. Chem.* **2021,** 214, 113204.

25. Lovering, F.; Bikker, J.; Humblet, C. Escape from Flatland: Increasing Saturation as an Approach to Improving Clinical Success. *J. Med. Chem.* **2009,** 52, 6752-6756.

26. Wei, W.; Cherukupalli, S.; Jing, L.; Liu, X.; Zhan, P. Fsp3: A New Parameter for Drug-likeness. *Drug Discov. Today* **2020,** 25, 1839-1845.

27. Wang, J.; Liu, H. Lead Compound Optimization Strategy (1)--Changing Metabolic Pathways and Optimizing Metabolism Stability. *Yao Xue Xue Bao* **2013,** 48, 1521-1531.

28. Zhou, H.-J.; Wang, J.; Yao, B.; Wong, S.; Djakovic, S.; Kumar, B.; Rice, J.; Valle, E.; Soriano, F.; Menon, M.-K.; Madriaga, A.; Kiss von Soly, S.; Kumar, A.; Parlati, F.; Yakes, F. M.; Shawver, L.; Le Moigne, R.; Anderson, D. J.; Rolfe, M.; Wustrow, D. Discovery of a First-in-Class, Potent, Selective, and Orally Bioavailable Inhibitor of the p97 AAA ATPase (CB-5083). *J. Med. Chem.* **2015,** 58, 9480-9497.

29. Kang, D.; Fang, Z.; Huang, B.; Lu, X.; Zhang, H.; Xu, H.; Huo, Z.; Zhou, Z.; Yu, Z.; Meng, Q.; Wu, G.; Ding, X.; Tian, Y.; Daelemans, D.; De Clercq, E.; Pannecouque, C.; Zhan, P.; Liu, X. Structure-Based Optimization of Thiophene[3,2-d]pyrimidine Derivatives as Potent HIV-1 Non-nucleoside Reverse Transcriptase Inhibitors with Improved Potency against Resistance-Associated Variants. *J. Med. Chem.* **2017,** 60, 4424-4443.

30. Zhang, H.; Tian, Y.; Kang, D.; Huo, Z.; Zhou, Z.; Liu, H.; De Clercq, E.; Pannecouque, C.; Zhan, P.; Liu, X. Discovery of Uracil-bearing DAPYs Derivatives as Novel HIV-1 NNRTIs via Crystallographic Overlay-based Molecular Hybridization. *Eur. J. Med. Chem.* **2017,** 130, 209-222.

31. Riggs, J. R.; Elsner, J.; Cashion, D.; Robinson, D.; Tehrani, L.; Nagy, M.; Fultz, K. E.; Krishna Narla, R.; Peng, X.; Tran, T.; Kulkarni, A.; Bahmanyar, S.; Condroski, K.; Pagarigan, B.; Fenalti, G.; LeBrun, L.; Leftheris, K.; Zhu, D.; Boylan, J. F. Design and Optimization Leading to an Orally Active TTK Protein Kinase Inhibitor with Robust Single Agent Efficacy. *J. Med. Chem.* **2019,** 62, 4401-4410.

32. Tan, L.; Zhang, Z.; Gao, D.; Luo, J.; Tu, Z.-C.; Li, Z.; Peng, L.; Ren, X.; Ding, K. 4-Oxo-1,4-dihydroquinoline-3-carboxamide Derivatives as New Axl Kinase Inhibitors. *J. Med. Chem.* **2016,** 59, 6807-6825.

33. Huang, B.; Liu, X.; Li, W.; Chen, Z.; Kang, D.; Zhan, P.; Liu, X. An Improved Synthesis Approach of the HIV-1 Inhibitor RDEA427, a Pyrrolo[2,3-d]pyrimidine Derivative. *ARKIVOC* **2016,** 2016, 45-51.

34. Pannecouque, C.; Daelemans, D.; De Clercq, E. Tetrazolium-based Colorimetric Assay for the Detection of HIV Replication Inhibitors: Revisited 20 Years Later. *Nat. Protoc.* **2008,** 3, 427-434.

35. Kang, D.; Ruiz, F. X.; Sun, Y.; Feng, D.; Jing, L.; Wang, Z.; Zhang, T.; Gao, S.; Sun, L.; De Clercq, E.; Pannecouque, C.; Arnold, E.; Zhan, P.; Liu, X. 2,4,5-Trisubstituted Pyrimidines as Potent HIV-1 NNRTIs: Rational Design, Synthesis, Activity Evaluation, and Crystallographic Studies. *J. Med. Chem.* **2021,** 64, 4239-4256.

36. Wang, Z.; Yu, Z.; Kang, D.; Zhang, J.; Tian, Y.; Daelemans, D.; De Clercq, E.; Pannecouque, C.; Zhan, P.; Liu, X. Design, Synthesis and Biological Evaluation of Novel Acetamide-substituted Doravirine and Its Prodrugs as Potent HIV-1 NNRTIs. *Bioorg. Med. Chem.* **2019,** 27, 447-456.

37. Huang, B.; Liang, X.; Li, C.; Chen, W.; Liu, T.; Li, X.; Sun, Y.; Fu, L.; Liu, H.; De Clercq, E.; Pannecouque, C.; Zhan, P.; Liu, X. Fused Heterocycles Bearing Bridgehead Nitrogen as Potent HIV-1 NNRTIs. Part 4: Design, Synthesis and Biological Evaluation of Novel Imidazo[1,2-a]pyrazines. *Eur. J. Med. Chem.* **2015,** 93, 330-337.

38. Leeson, P. D.; Springthorpe, B. The Influence of Drug-like Concepts on Decision-making in Medicinal Chemistry. *Nat. Rev. Drug Discov.* **2007,** 6, 881-890.

39. Hopkins, A. L.; Keserü, G. M.; Leeson, P. D.; Rees, D. C.; Reynolds, C. H. The Role of Ligand Efficiency Metrics in Drug Discovery. *Nat. Rev. Drug Discov.* **2014,** 13, 105-121.

40. Abad-Zapatero, C. Ligand Efficiency Indices for Effective Drug Discovery. *Expert Opin. Drug Discov.* **2007,** 2, 469-488.

41. Yang, Y.; Kang, D.; Nguyen, L. A.; Smithline, Z. B.; Pannecouque, C.; Zhan, P.; Liu, X.; Steitz, T. A. Structural Basis for Potent and Broad Inhibition of HIV-1 RT by Thiophene[3,2-d]pyrimidine Non-nucleoside Inhibitors. *eLife* **2018,** 7, e36340.

42. Kang, D.; Zhang, H.; Wang, Z.; Zhao, T.; Ginex, T.; Luque, F. J.; Yang, Y.; Wu, G.; Feng, D.; Wei, F.; Zhang, J.; De Clercq, E.; Pannecouque, C.; Chen, C. H.; Lee, K.-H.; Murugan, N. A.; Steitz, T. A.; Zhan, P.; Liu, X. Identification of Dihydrofuro[3,4-d]pyrimidine Derivatives as Novel HIV-1 Non-Nucleoside Reverse Transcriptase Inhibitors with Promising Antiviral Activities and Desirable Physicochemical Properties. *J. Med. Chem.* **2019,** 62, 1484-1501.

43. Kang, D.; Feng, D.; Ginex, T.; Zou, J.; Wei, F.; Zhao, T.; Huang, B.; Sun, Y.; Desta, S.; De Clercq, E.; Pannecouque, C.; Zhan, P.; Liu, X. Exploring the Hydrophobic Channel of NNIBP Leads to the Discovery of Novel Piperidine-substituted Thiophene[3,2-d]pyrimidine Derivatives as Potent HIV-1 NNRTIs. *Acta Pharmaceutica Sinica B* **2020,** 10, 878-894.

44. Frey, K. M.; Puleo, D. E.; Spasov, K. A.; Bollini, M.; Jorgensen, W. L.; Anderson, K. S. Structure-Based Evaluation of Non-nucleoside Inhibitors with

Improved Potency and Solubility That Target HIV Reverse Transcriptase Variants. *J. Med. Chem.* **2015,** 58, 2737-2745.

45. Feng, M.; Wang, D.; Grobler Jay, A.; Hazuda Daria, J.; Miller Michael, D.; Lai, M.-T. In Vitro Resistance Selection with Doravirine (MK-1439), a Novel Nonnucleoside Reverse Transcriptase Inhibitor with Distinct Mutation Development Pathways. *Antimicrob. Agents Chemother.* **2014,** 59, 590-598.
46. Lai, M.-T.; Feng, M.; Falgueyret, J.-P.; Tawa, P.; Witmer, M.; DiStefano, D.; Li, Y.; Burch, J.; Sachs, N.; Lu, M.; Cauchon, E.; Campeau, L.-C.; Grobler, J.; Yan, Y.; Ducharme, Y.; Côté, B.; Asante-Appiah, E.; Hazuda Daria, J.; Miller Michael, D. In Vitro Characterization of MK-1439, a Novel HIV-1 Nonnucleoside Reverse Transcriptase Inhibitor. *Antimicrob. Agents Chemother.* **2014,** 58, 1652-1663.
47. Molina, J.-M.; Squires, K.; Sax, P. E.; Cahn, P.; Lombaard, J.; DeJesus, E.; Lai, M.-T.; Xu, X.; Rodgers, A.; Lupinacci, L.; Kumar, S.; Sklar, P.; Nguyen, B.-Y.; Hanna, G. J.; Hwang, C.; Martins, M.; Cahn, P. E.; Lopardo, G. D.; Porteiro, N.; Bloch, M. T.; Baker, D. A.; Roth, N.; Moore, R. J.; Finlayson, R. J.; McMahon, J.; Rieger, A.; Zoufaly, A.; Hartl, S.; Zangerle, R.; Smaill, F.; Walmsley, S. L.; Conway, B.; Rachlis, A.; Smith, G. H. R.; Perez, C.; Afani, A.; Campos Barker, M. I. E.; Chahin, C. E.; Wolff Reyes, M.; Gerstoft, J.; Weis, N.; Laursen, A. L.; Molina, J.-M.; Yazdanpanah, Y.; Cotte, L.; Raffi, F.; Morlat, P.; Girard, P.-M.; Katlama, C.; Rockstroh, J. K.; Arasteh, K.; Esser, S.; Stoehr, A.; Stellbrink, H.-J.; Stoll, M.; Schuermann, D.; Faetkenheuer, G.; Bogner, J.; Lutz, T.; Baumgarten, A.; Jaeger, H.; Gori, A.; Coltan, G.; Constandis, F.; Erscoiu, S. M.; Prisacariu, L.-J.; Rugina, S.; Streinu-Cercel, A.; Pokrovsky, V. V.; Zakharova, N. V.; Shuldyakov, A. A.; Ryamova, E. P.; Kulagin, V. V.; Tsybakova, O. A.; Orlova-Morozova, E.; Nagimova, F.; Voronin, E.; Shimonova, T. E.; Kozyrev, O. A.; Orrell, C.; Lombaard, J. J.; Botes, M. E.; Portilla, J.; Gatell, J. M.; Perez, M. J.; Arribas, J. R.; Negredo, E.; Podzamczer, D.; Pulido, F.; Troya, J.; De los Santos, I.; Berenguer, J.; Williams, I. G.; Johnson, M. A.; Schembri, G.; Clarke, A.; Gompels, M.; Fox, J. M.; Taylor, S. J.; Kegg, S.; Hagins, D. P.; Osiyemi, O. O.; Prelutsky, D. J.; Ramgopal, M. N.; Dretler, R.; DeJesus, E.; Sloan, L.; Lewis, S. T.; Clay, P. G.; Bellos, N. C.; Thompson, M. A.; Montero, J.; McDonald, C. K.; Creticos, C.; Shamblaw, D.; Terrelonge, A. E.; Valdes, M.; Tashima, K. T.; Robbins, W. J.; Felizarta, F. A.; Elion, R. A.; Slim, J.; Lalezari, J. P.; Lalla-Reddy, S. N.; Ruane, P. J.; Mills, A.; Cade, J. L.; Campo, R. E.; Dietz, C. A.; Blick, G.; Mayer, C.; Rondon, J. C.; Cook, P. P.; Daar, E.; Kumar, P. N.; Swindells, S.; Castro, J. G.; Morales-Ramirez, J. O.; Santiago, L.; Santana-Bagur, J. L. Doravirine versus Ritonavir-boosted Darunavir in Antiretroviral-naive Adults with HIV-1 (DRIVE-FORWARD): 48-Week Results of a Randomised, Double-blind, Phase 3, Non-inferiority trial. *The Lancet HIV* **2018,** 5, e211-e220.
48. Orkin, C.; Squires, K. E.; Molina, J.-M.; Sax, P. E.; Wong, W.-W.; Sussmann, O.; Kaplan, R.; Lupinacci, L.; Rodgers, A.; Xu, X.; Lin, G.; Kumar, S.; Sklar, P.; Nguyen, B.-Y.; Hanna, G. J.; Hwang, C.; Martin, E. A.; Group, D.-A. S.

Doravirine/Lamivudine/Tenofovir Disoproxil Fumarate is Non-inferior to Efavirenz/Emtricitabine/Tenofovir Disoproxil Fumarate in Treatment-naive Adults With Human Immunodeficiency Virus–1 Infection: Week 48 Results of the DRIVE-AHEAD Trial. *Clin. Infect. Dis.* **2019,** 68, 535-544.

49. Smith, S. J.; Pauly, G. T.; Akram, A.; Melody, K.; Ambrose, Z.; Schneider, J. P.; Hughes, S. H. Rilpivirine and Doravirine Have Complementary Efficacies Against NNRTI-Resistant HIV-1 Mutants. *J. Acquir. Immune. Defic. Syndr.* **2016,** 72, 485-491.

50. Huang, B.; Liu, X.; Tian, Y.; Kang, D.; Zhou, Z.; Daelemans, D.; De Clercq, E.; Pannecouque, C.; Zhan, P.; Liu, X. First Discovery of a Potential Carbonate Prodrug of NNRTI Drug Candidate RDEA427 with Submicromolar Inhibitory Activity against HIV-1 K103N/Y181C Double Mutant Strain. *Bioorg. Med. Chem. Lett.* **2018,** 28, 1348-1351.

Table of Contents Graphic